INVESTIGATION OF QUANTITATIVE NMR BY STATISTICAL ANALYSIS

INVESTIGATION OF QUANTITATIVE NMR BY STATISTICAL ANALYSIS

By

LYDIA LAI-MUI LAO, B.Sc.

A Thesis

submitted to the School of Graduate Studies

in Partial Fulfilment of the Requirements

for the Degree

Master of Science

McMaster University

MASTER OF SCIENCE (1991) McMASTER UNIVERSITY
(Chemistry) Hamilton, Ontario

TITLE: Investigation of Quantitative NMR by Statistical Analysis

AUTHOR: Lydia Lai-Mui Lao, B.Sc. (McMaster University)

SUPERVISOR: Professor A. D. Bain

NUMBER OF PAGES: xi, 88

" To everything there is a season,
and a time to every purpose under the heaven. "

TO

MY PARENTS

WITH LOVE

and

TO GOD

MAY ALL THE PRAISES BE

ABSTRACT

Quantitation by nuclear magnetic resonance (NMR) has been frequently done with integrals. The use of peak heights has been thought to be unreliable. The aim of this thesis is to examine the reliability of peak height method in achieving quantitative NMR measurements for small molecules such as water and sucrose.

Isotope measurements have been traditionally done by isotope-ratio mass spectrometry. This is no doubt a highly sensitive technique for analyzing pure samples but the analysis of mixtures is not as straight-forward as it would be for the former. Ontario Hydro has encountered problems in measuring deuterium in DMSO/water mixtures. To solve the problem with NMR, an analytical method has been established to measure the deuterium content in waters and in DMSO/water mixtures. This involved testing a linear model for analyzing waters which were enriched or depleted with deuterium as well as applying the model to quantify DMSO/water mixtures. Both ^{1}H and ^{2}H NMR were employed. Satisfactory accuracy and precision of the results were obtained.

For quantitative ^{13}C work, the peak height method is often not recommended due to the variations in signal width, which is a result of varied T_2 values and nuclear Overhauser enhancement (NOE). Sucrose molecules in cane sugar and beet sugar have different ^{13}C isotopic ratios because they are synthesized by different photosynthetic

pathways. To see the usefulness and limitation of the peak height method, ^{13}C spectra of sucrose were acquired and the carbon peaks were quantified. Good precision was achieved but no predictable trend in the isotope difference could be found.

ACKNOWLEDGEMENTS

I would like to express my gratitude to my supervisor, Dr. A.D. Bain, who has supervised the research and been tortured by my ignorance from the very beginning till the end of the work. Without his great belief in NMR, in particular the simple pulse sequence technique, this work would not have been completed. It is his respect towards students and his willingness to help and guide that are most appreciated.

I am also grateful to have Mr. I. Burton, Ms. J. Cramer, Dr. B. Fulton, Mr. S. Hughes and Mr. G. Duns in the research group. Their gentleness and laughter often filled the work place with warmth. Special thanks are due to Mr. I. Burton whose computer knowledge helped in most the time I needed. The assistance of Mr. B. Sayer and Dr. D.W. Hughes in getting me acquainted to the NMR spectrometers and in solving many of the operating problems are also acknowledged.

I wish to thank Mr. Y.-B. Ip who advised me to study abroad and supported me financially in the undergraduate years. Sincerely I thank the brothers and sisters in H.C.C.F. who supported me through prayer and encouragement. Wordless thanks are especially due to Manda Li for her endless patience, understanding and care has sustained me through times of difficulties.

Finally, it is to God and to my family that all my gratitude be.

TABLE OF CONTENTS

LIST OF TABLES

LIST OF FIGURES

CHAPTER 1 INTRODUCTION

Nuclear magnetic resonance (NMR) spectroscopy[1-5] has been undergoing explosive development in recent years. It has become one of the most powerful analytical techniques in elucidating and identifying molecular structures, and in studying molecular dynamics.[6,7] With the two-dimensional[8,9] and imaging techniques,[10-13] and the discovery of multiple-pulse sequences,[14] larger molecules and complicated systems such as human organs are able to be resolved. The growth of the use of NMR in polymer chemistry, pharmaceutical applications, biological and biomedical area[15-21] marks the diversity of the technique.

There are certain advantages of NMR. The primary advantage is that it can be applied to common isotopes such as proton (^{1}H) and carbon-13 (^{13}C). Protons exist in the majority of compounds while carbon forms the backbone of all organic compounds.[22] In other words, many samples that have analytical value are potentially NMR-active. In fact, ^{1}H and ^{13}C NMR are now routine operations in NMR laboratories for analytical purposes.[7, 23-26] Other isotopes such as ^{19}F, ^{31}P, ^{2}H and ^{15}N are also frequently studied by NMR methods.[27-32]

NMR is known for its high selectivity because it is isotope-specific. Only one nucleus is observed at the specified resonance frequency and hence separation of a nucleus from its isotopes or other co-existing NMR-active nuclei is not required. NMR

also provides information about a specific site of a molecule whether this site is isotope-enriched or -depleted and how much enrichment or depletion it encounters.

Handling of samples is straight-forward. A sample is simply put in an NMR tube and unlike mass spectroscopy, no degradation of sample prior to spectroscopic analysis is needed. NMR is also non-destructive. A sample will be preserved after running NMR spectra and for this reason, further analysis is possible. More importantly, sensitivity can be enhanced by accumulating many scans because the sample can be re-used. The problem of cross-contamination is minimized for samples are individually contained in tubes. In the case where a standard material is employed to be a reference, specially-designed coaxial or concentric tubes[33,34] can be used to separate the reference and the sample.

Quantitative measurements are relatively direct and simple. The reason is that NMR signal intensity is directly proportional to the number of nuclei present in a sample. Therefore, if given an NMR spectrum of good signal-to-noise ratio (S/N), the composition of a mixture or the concentration of an unknown can be found by measuring the signal intensity.

The major disadvantage of quantitation by NMR compared to many other spectroscopic methods is the inherently low sensitivity. NMR measures the population difference between energy levels which is one in 10^5 for protons in a magnetic field of 2.3 Tesla (100 MHz). For low-abundance nuclei like deuterium, the sensitivity is even lower. Milligrams or grams of sample, depending on molecular weight, are often required to obtain a spectrum with good S/N ratio. However, the discovery of the pulsed

techniques[35-38] together with the use of Fourier transformation[39,40] and superconducting high-field magnets, and the advances in computer technology[41] have greatly improved the sensitivity and resolution. Specifically, the capability to carry out signal averaging in reasonably short time periods does compensate for the low sensitivity. Moreover, the development of multinuclear probes facilitates the use of ^{7}Li, ^{11}B, ^{17}O, ^{27}Al, ^{29}Si, ^{39}K, and ^{129}Xe in laboratory work.[6,7]

Throughout the years, extensive work has been done employing the qualitative aspects of NMR. Yet, the power of NMR in quantifying a spectrum has not been fully explored. Some principles in dealing with quantitation by ^{1}H NMR had been laid down by workers who were devoted to topics on analytical NMR in the 1970's.[42,43] It was not until 1974 that Shoolery discussed in detail the consideration for getting quantitative measurements in ^{13}C NMR.[44,45] Reviews and topics on quantitative ^{1}H and ^{13}C NMR gradually appeared in the literature.[46-49,24] In this literature integrals are almost always used in quantitation.

It is well-accepted that integration is a reliable quantitation method in NMR. The use of peak height has received relatively little interest in the past. In recent years, the development of the site-specific natural isotope fractionation (SNIF) method by Martin *et al.*[50-53] has opened a new area of NMR in quantitative aspect. In their work, quantitative deuterium (^{2}H) NMR is used to characterize the origin and to study the chemical and biochemical mechanisms of natural products in alcoholic beverages and food products. Relative peak heights are used to quantify the spectrum. Not only the accuracy but also the precision of the data and the method have been widely

examined.[54,55] Applications were also made on studies of deuterium kinetic isotope effects.[56-58]

Undoubtedly, integrals are accurate due to the direct proportionality to the total number of spins present in a sample. Nevertheless, precautions have to be taken in order to obtain accurate and reproducible integral. These have been thoroughly discussed in the papers written by Shoolery, Gillet and Delpuech, and Sotak *et al.*[44,45,48,59-61] However, using integrals inevitably involves subjective factors which might lead to serious errors in the precision of the results.[62] On the other hand, the major drawback of using peak height is variation in linewidth and lineshape[42,43] which depends mostly on instrumental parameters. Provided that the variation can be eliminated, peak height is in fact very reproducible.[63-67] In the case of quadrupolar nuclei where effects on linewidths are minimal, the peak height method is very accurate if signals are not too broad.[68]

It is an attempt in this thesis to see whether quantitative measurements by the peak height method can be made within accepted analytical precision. With the use of statistical analysis, it is hoped that the quality of the NMR data can be presented in an honest manner.

A brief review of basic NMR theory is found in Chapter 2. Particular emphasis is put on relaxation and the nuclear Overhauser effect (NOE) which are two important factors affecting quantitative measurements. Chapter 3 is devoted to the quantitation method. The strength and weakness of integrals and peak heights and eventually the reasons for using peak heights are presented followed by a discussion on data analysis. The chapter is ended by a list of consideration for NMR experiments.

The main objective of the experiments is to see how effective NMR can be as a tool for quantitation in analytical chemistry. This involves establishing a method with an analytical precision acceptable within experimental and instrumental errors. Once the method has been validated, further experiments then reveal the applicability of the method in analytical areas. The experiments were done along two main streams: 1. measuring ^{2}H quantitatively in deuterium-enriched or -depleted waters and in DMSO/water mixtures and; 2. measuring ^{13}C in sucrose in sugars synthesized by different photosynthetic pathways. ^{2}H, ^{13}C and ^{1}H NMR were employed. The experimental details and results are found in Chapter 4 and 5. Chapter 4 focuses on the water experiments whereas Chapter 5 focuses on the ^{13}C work which consists of sugar and sugar octaacetate experiments. Finally, Chapter 6 concludes the whole thesis.

CHAPTER 2 THEORY

The objective of this chapter is to outline the basic principles of pulsed Fourier transform (FT) NMR. This is not to include extensive discussion of every aspect nor detailed derivation of equations. These can be found in the literature. NMR makes use of the existing discrete energy levels of spin systems. Thus, the principles lie on how to perturb the spin system to produce observable and measurable signals. That is, the properties of a nucleus, the perturbation and the response are to be elaborated. General references can be found in Ref. 1, 3 and 69.

2.1 Basic Principles

In 1924, Pauli first suggested that certain atomic particles behave like a spinning electric charge and possess angular momentum.[70] As predicted by electrodynamics, they behave like magnetic dipoles and have magnetic moments (μ). These nuclei are said to have a spin. Nuclear angular momentum is quantized and the number of observable spin states is determined by the spin quantum number, I. I is a half-integer if the mass number (A) of the nucleus is odd, an integer if the atomic number (Z) is odd and A is even, and I = 0 if both A and Z are even. When $I \geq 1/2$, the nucleus also possesses a quadrupole moment.

In quantum mechanical terms, when a nucleus is placed in an applied magnetic field ($\mathbf{B_o}$), the spin will be split into (2I+1) energy levels which are characterized by the nuclear spin quantum number, m_I. Since the proton (^1H) and carbon-13 (^{13}C) have spin 1/2, there will be in both cases two energy levels, namely, m_I = +1/2, -1/2 (**Figure 1**). Deuterium (^2H) has spin 1 and therefore three energy levels are possible, namely, m_I = +1, 0, -1. The allowed energy levels are field dependent,

$$E = -\mu \cdot B_o$$
$$= -\frac{h\gamma m_I B_o}{2\pi} \qquad (1)$$

where μ is the magnetic moment, **Bo** is the applied magnetic field, h is the Planck's constant and γ is the gyromagnetic ratio which is specific to the observed nucleus. Transitions are subject to the selection rule Δm_I = +/-1. Thus the separation of adjacent energy levels is

$$\Delta E = \frac{h\gamma B_o}{2\pi} \qquad (2)$$

The corresponding observation frequency is

$$\nu_o = \frac{\gamma B_o}{2\pi} \qquad (3)$$

$$\omega_o = \gamma B_o \qquad (4)$$

This indicates that under the influence of an external magnetic field, μ will precess about $\mathbf{B}_0$ at a frequency of ν_0 which is termed the Larmor frequency.

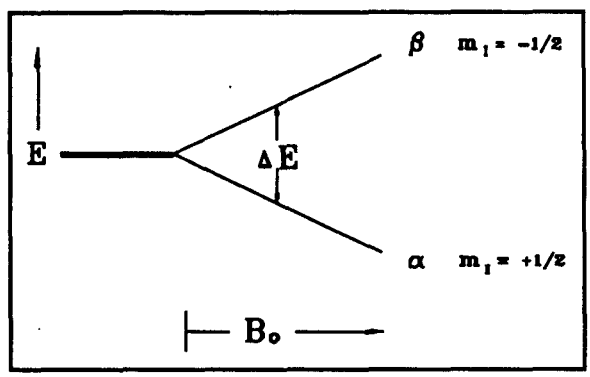

Figure 1. Energy levels of a spin-1/2 nucleus. Energy difference increases with increasing magnetic field.

In terms of classical description, a spin is like a bar magnet. When this spin is placed in a magnetic field, its magnetic moment aligns with the external field. Since the spin is also an angular momentum, a torque is generated by the magnet on the rotational motion of the nucleus. The interaction between this rotational torque and the magnetic moment causes μ to precess about $\mathbf{B}_0$ at the Larmor frequency ν_0.

Taking the proton as an example, the population ratio between the two energy states α ($m_I = +1/2$) and β ($m_I = -1/2$) is governed by the Boltzmann distribution

$$\frac{N_\alpha}{N_\beta} = \exp\left(\frac{-\Delta E}{kT}\right) \qquad (5)$$

in which the population in the lower energy state, α, is in small excess. The population difference is $\approx \Delta E/kT$. At room temperature in a field of 2.35 Tesla, ΔE in frequency term is 100 MHz and kT is ~ 6×10^6 MHz. The Boltzmann excess is therefore 1 in 10^5 protons.

Macroscopically, if the magnetization across the whole sample resulting from the population difference is viewed as a vector sum of all magnetic dipoles in the sample, this sum, **M**, aligns with $\mathbf{B}_o$ (z-axis) at thermal equilibrium and is proportional to the population difference of the two energy states (**Figure 2**). To perturb the spin system, a time-dependent radiofrequency (RF) field, $\mathbf{B}_1$, or a pulse is applied perpendicular to $\mathbf{B}_o$. This causes **M** to flip away from $\mathbf{B}_o$, producing a longitudinal (z) component ($\mathbf{M}_z$) and a transverse (xy) component ($\mathbf{M}_{xy}$) which represents the net xy magnetization in the xy-plane. Resonance

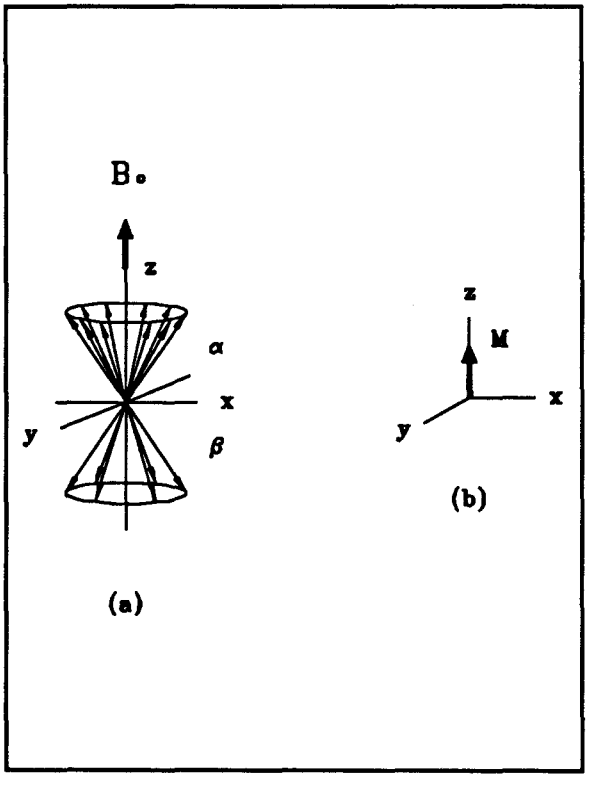

Figure 2. Vector presentation of population distribution of a spin-1/2 nucleus. (a) spin coherence; (b) macroscopic sum.

is said to occur. An effective field is set up in the rotating frame

$$B_{eff} = B_o + B_1 + \frac{\omega}{\gamma}$$
$$= \frac{\omega_o - \omega}{\gamma} + B_1 \qquad (6)$$

where $\mathbf{B}_{eff}$ is the resultant vector of $\mathbf{B}_1$ and the reduced static field, $(\omega_o-\omega)/\gamma$. The term ω/γ is called the fictitious field which is a result of a change in coordinate systems (**Figure 3**). For the case where $\omega = \omega_o$, $\mathbf{B}_{eff}$ reduces to $\mathbf{B}_1$ and **M** will precess about $\mathbf{B}_1$ as long as the pulse is on. This is the on-resonance condition. Otherwise, off-resonance occurs and **M** will precess about $\mathbf{B}_{eff}$. The angle of displacement depends on the strength of $\mathbf{B}_1$ and is equal to $\gamma B_1 t_p$ where t_p is the duration of the pulse. When $\mathbf{B}_1$ is off, $\mathbf{M}_z$ gradually returns to its equilibrium value and $\mathbf{M}_{xy}$ decays to zero via various relaxation mechanisms. An NMR signal is detected in the form of oscillating current induced by the decaying $\mathbf{M}_{xy}$ by a receiver coil wound about an axis perpendicular to $\mathbf{M}_o$. This signal is called a free induction decay (FID). The time-domain FID is Fourier transformed into a frequency-domain NMR spectrum to obtain information necessary for quantitative analysis.

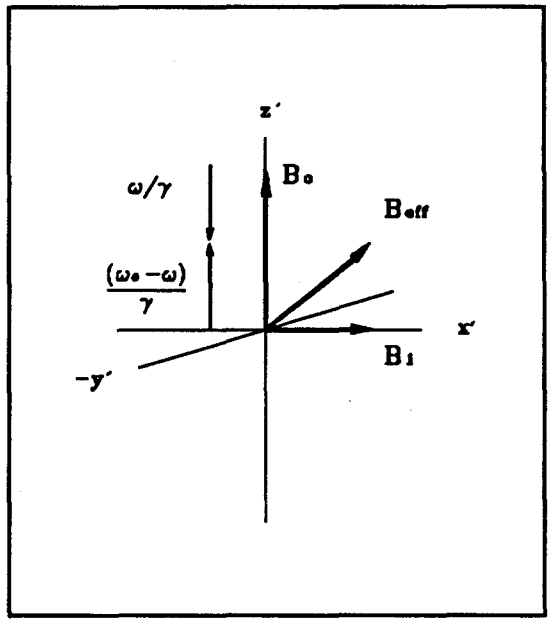

Figure 3. The effective field, $\mathbf{B}_{eff}$, in the rotating frame.

2.2 Relaxation

When a spin system is subjected to a pulse, the population excess is promoted to the higher energy level, β. After the pulse is removed, magnetizations are assumed to recover through first-order exponential processes. They are called spin-lattice (longitudinal) and spin-spin (transverse) relaxation corresponding respectively to the decay of $\mathbf{M}_z$ and $\mathbf{M}_{xy}$. The former is an enthalpy process whereas the latter is an entropy process.

Spin-lattice relaxation is described by the equation

$$M_z - M_o = (M_z^{ini} - M_o) \exp(-t/T_1) \tag{7}$$

where M_z^{ini} and M_o are the initial and equilibrium z-magnetization respectively, t is the time variable and T_1 is the spin-lattice relaxation time constant characteristic of the time for the Boltzmann excess to be restored. It is M_z whose magnitude is observed.

The T_1 value is characteristic of the type of nucleus and its environment. It ranges from microseconds to hours, depending on factors such as temperature, viscosity, molecular size and physical state of the molecule. For protons and carbons in solution, T_1s are in the range of 0.1-100 sec. For quantitative experiments, a sufficient recycle time is needed for M_z to relax to equilibrium before next pulse is applied. This requires at least 5 T_1[71] to be put between pulses so that at least 99.3 % of the magnetization can be recovered. Thus, T_1 of the observed nucleus must be estimated.

There are several factors which contribute to T_1 relaxation. The important ones are intramolecular dipole-dipole relaxation, quadrupolar relaxation and intermolecular dipole-dipole (paramagnetic) relaxation. For spin-1/2 nuclei such as proton and carbon, the presence of fluctuating magnetic fields due to the tumbling of neighbouring magnetic dipoles (e.g. protons) induces a transition pathway for the other (carbon) spins. They interact through dipolar interactions and the excess energy is eventually passed to the lattice. For $I \geq 1/2$ nuclei such as deuterium, the presence of fluctuating electric fields due to non-symmetric electronic environment (electric field gradient) enables these spins to relax through quadrupolar relaxation. The presence of unpaired electrons in some paramagnetic substances also provide a good means for the spins to relax because such substances have large magnetic moment and induce rapid relaxation.

In addition to the T_1 process, spin-spin relaxation characterized by the T_2 time

constant is another relaxation pathway. The shorter T_1 and T_2 the more efficient relaxation is. During spin-spin relaxation, the phase coherence of the xy magnetizations is gradually lost and T_2 is the time the net xy magnetization (M_{xy}) decays to zero. It is important to note that T_2 is inversely related to the signal width which is a prime factor determining the use of peak height in quantitation. In real life experiments, natural linewidth resulting solely from T_2 process is seldom obtained. Other factors such as magnetic homogeneity and the decoupler efficiency also contribute to the dephasing process. Consequently, an effective time constant (T_2^*) is observed instead of T_2.

2.3 Nuclear Overhauser Effect (NOE)[72]

Nuclear Overhauser effect (NOE) is a phenomenon involving a change in intensity of an NMR resonance when a second resonance is saturated by irradiation of an RF pulse. NOE can occur in homonuclear or heteronuclear spin systems. Since the ^{13}C experiments done for this thesis employed proton-decoupling, heteronuclear NOE using simple two-spin system will be discussed.

If a signal has normal intensity A_o and observed intensity A, then NOE is defined as

$$\eta_I(S) = \frac{A - A_o}{A_o} \qquad (8)$$

I is the spin being observed while S is the one being saturated. **Figure 4a** depicts a two-spin system labelled with energy states $\alpha\alpha$, $\alpha\beta$, $\beta\alpha$ and $\beta\beta$ of spins I and S. The transitions are denoted by the various transition probabilities W_o, W_1 and W_2. At thermal equilibrium, the Boltzmann distribution results in a net population excess in $\alpha\alpha$ state. Population differences are seen in W_1 (single quantum) and W_2 (double quantum) transitions. The population difference in W_o (zero quantum) transition is very small because $\alpha\beta$ and $\beta\alpha$ are very close in energy and it is often negligible. When S resonance is saturated, the populations in $\alpha\alpha$ and $\beta\alpha$, and in $\alpha\beta$ and $\beta\beta$ are equalized, forcing the overall population to rearrange among different energy states (**Figure 4b**). At this point, no intensity change of I transitions is observed since the population difference involving I transitions remain unchanged. However, the population difference in $\alpha\alpha$-$\beta\beta$ and $\alpha\beta$-$\beta\alpha$ transitions are altered. The system tends to return to thermal equilibrium. Relaxation of both spins through W_2 transition pathway transfers the population from $\beta\beta$ to $\alpha\alpha$, causing a decrease in $\alpha\beta$ population and an increase in $\beta\alpha$ population, resulting in an overall increase in I intensity and hence a positive NOE enhancement is said to be produced (**Figure 4c**). Similarly, mutual spin-flip of both spins through the W_o transition brings population from $\beta\alpha$ to $\alpha\beta$, causing an increase in $\beta\beta$ population and a decrease in $\alpha\alpha$ population and hence producing a negative NOE (**Figure 4d**).

Since W_1 requires a magnetic field fluctuating at ν_o (10^8-10^9 Hz) and W_2 at $2\ \nu_o$, relaxation through these transitions is most efficient for small, fast tumbling molecules in non-viscous solution. On the other hand, W_o requires a low-frequency field and therefore it is most efficient for large, slow-tumbling molecules.

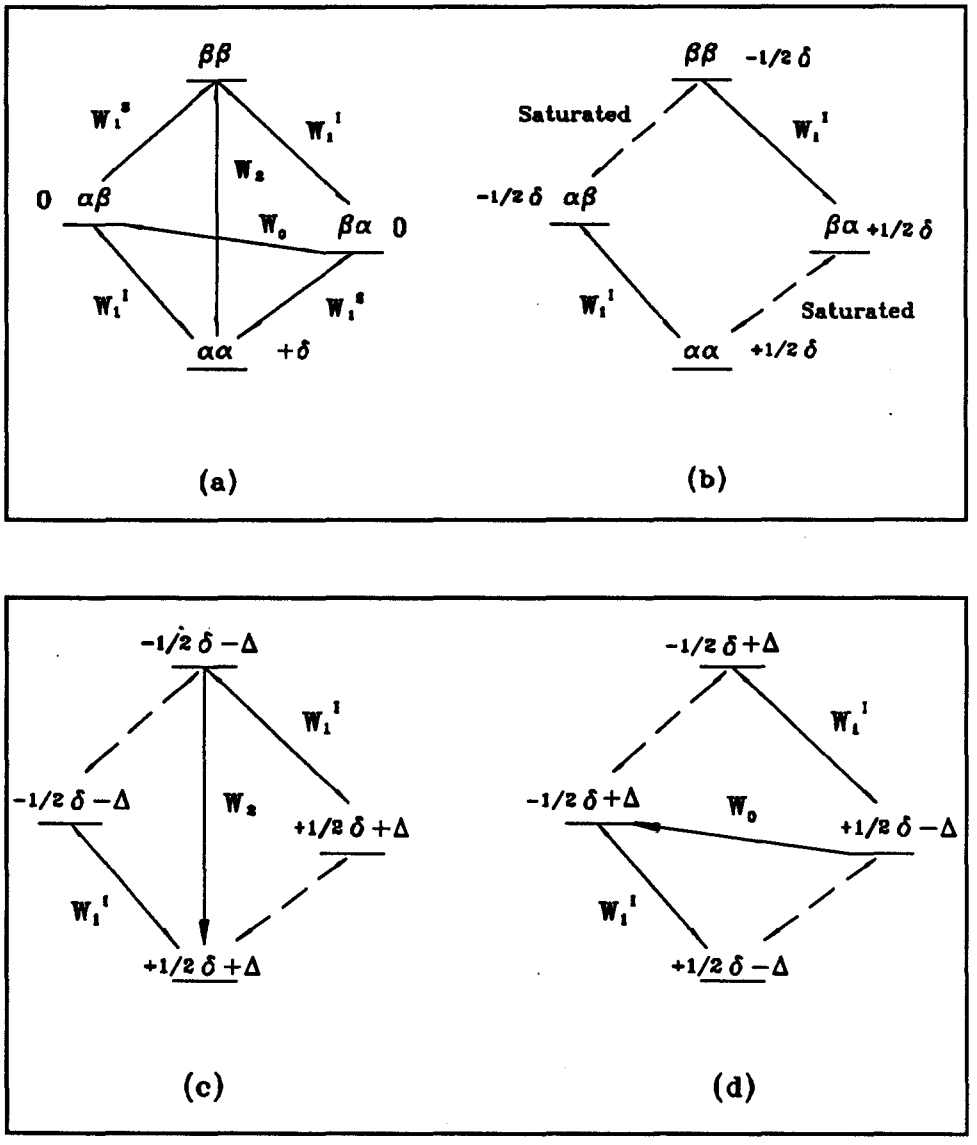

Figure 4. NOE effects on the population distribution of a heteronuclear spin system: (a) overall population difference arbitrarily assigned 2δ; (b) Saturation of S transitions; (c) double quantum; and (d) zero quantum transitions.

Using Solomon's equations[73] (see Noggle and Schirmer for detailed derivations[74,75]), NOE enhancement can be expressed as

$$\eta_I(S) = \frac{\gamma_S}{\gamma_I} \frac{W_2 - W_o}{2W_1I + W_o + W_2} = \frac{\gamma_S}{\gamma_I} \frac{\sigma_{IS}}{\rho_{IS}} \tag{9}$$

The term σ_{IS} denotes the cross-relaxation rate constant between spins I and S that describes the rate of dipole-dipole transitions giving rise to an NOE enhancement. The term ρ_{IS} is the dipolar longitudinal relaxation rate constant for relaxation of spin I by S. Note that dipolar relaxation here refers to intramolecular dipole-dipole relaxation.

If dipolar interaction is the only T_1 relaxation mechanism, then at the extreme-narrowing limit (the usual case in non-viscous solutions), $\sigma_{IS} = 1/2\ \rho_{IS}$ and the maximum NOE enhancement is expressed by

$$\eta_{max} = \frac{\gamma_S}{2\gamma_I} \tag{10}$$

Hence, in a proton-decoupled ^{13}C spectrum, η_{max} of carbon signals is 1.98 which means a three-fold enhancement is possible.

In reality, there are other relaxation mechanisms competing with dipolar relaxation and they contribute to the W_1 transitions.[76] Using R_I^{DD} as the relaxation rate from pure dipolar relaxation of spin I and R_I^{Other} as contributions from other competing mechanisms, (9) becomes

$$\eta_{max} = \frac{\gamma_S}{\gamma_I} \frac{\sigma_{IS}}{R_I^{DD} + R_I^{Other}} \qquad (11)$$

Some of the competing mechanisms have been mentioned in §2.3, others include chemical shift anisotropy, spin rotation and scalar relaxation.

Quantitative measurements require genuine signal intensities. NOE must be suppressed before taking any meaningful measurement. As mentioned before, competitive relaxation mechanisms contribute to the W_1 transitions and reduce NOE. Therefore, one way to quench NOE is to add a paramagnetic substance such as a transition metal (Cr^{3+}, Mn^{2+} or Fe^{3+}) or dissolved molecular oxygen so as to induce intermolecular dipolar interactions.[77,45] This is very effective since γ(electron) is 1000 times larger than $\gamma(^1H)$. For nuclei dominated by quadrupolar relaxation, NOE is essentially negligible. ^{13}C experiments are usually done with proton-decoupling. The saturation effect[78] caused by broadband decoupling must be removed in order to suppress NOE. This can be done by using inverse-gated decoupling.[79] The pulse sequence is shown in **Figure 5**. The decoupler is turned on only during acquisition and it is gated off during the delay time so that any NOE built up during acquisition will die away before a second pulse is applied. Since NOE takes on the order of T_1 to die away, a long delay is needed.

In summary, precautions must be taken to obtain good quantitative results. Sufficient time must be put between pulses for the spin system to equilibrate. Variations of signal intensity due to NOE enhancement must be suppressed.

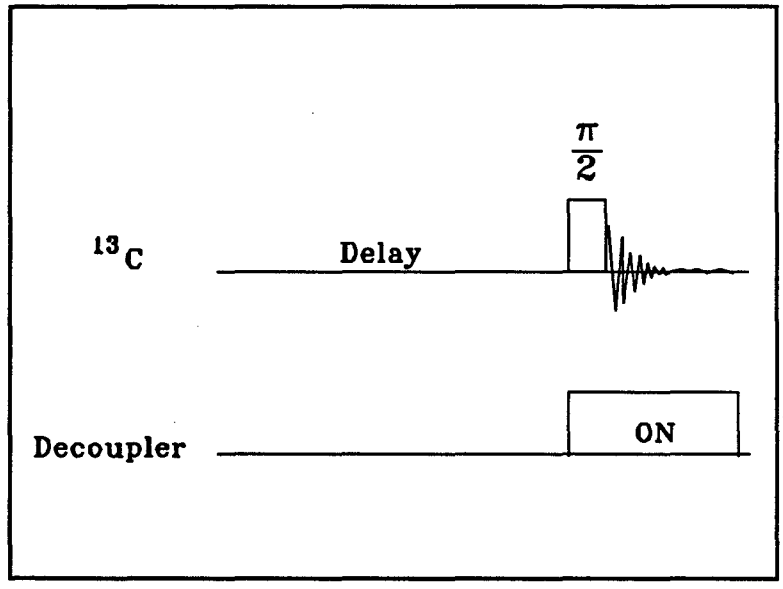

Figure 5. Pulse sequence for inverse gated-decoupling, the delay is set ≥ $5T_1$.

CHAPTER 3 QUANTITATION METHOD

NMR spectroscopy is good for quantitative measurements because of the direct proportionality of the signal intensities to the number of resonating nuclei. Quantitation methods which have been employed are basically measurement of chemical shift, peak width, peak area and peak height.[42,43] Among the four, peak area measurement is by far the most common and practical method in quantitative NMR.[48] As well, it is believed that area measurement is most reliable. The rest are reliable and to be used only under certain conditions. The work in this thesis is based on the measurements of peak heights and it is intended to show that quantitation by peak height measurement in fact is precise if careful considerations of the experimental design and data processing are taken. In the following sections, factors affecting quantitation measurements, the advantages and disadvantages of using peak area and peak heights, data analysis and consideration of NMR experiments will be discussed.

3.1 Factors Affecting Quantitative Measurements

3.1.1 Limitations of NMR

The major limitation of NMR to be an analytical tool is its inherent lack of sensitivity. The proton has been the most common nucleus being studied in the past due

to the fact that it has a large magnetic moment, has a high natural abundance and is present in almost all compounds. As mentioned before, the strength of an NMR signal depends on the population difference of the energy levels which corresponds to the Boltzmann distribution. The population difference depends on the gyromagnetic ratio, the magnetic field and the temperature. Tritium has the largest gyromagnetic ratio but it is not as versatile as the proton nuclei whose gyromagnetic ratio is the second largest. Therefore, under similar conditions, all other nuclei are less sensitive than proton. The natural abundance of ^{13}C is 1.108 % and that of ^{2}H is 0.015 %. The low natural abundance of these nuclei further lowers the sensitivity. If one wants to concentrate the sample solutions to compensate for the insensitivity, problems arising from the solubility limit and the availability of sample might be encountered.

Although the low sensitivity of NMR seems limiting, however, it can be compensated by adjusting instrumental parameters and taking precautions in data acquisition and data processing.

3.1.2 Instrumental Parameters

3.1.2.a Signal-to-noise ratio (S/N) and signal averaging

When an NMR signal is amplified, the background RF noise is also amplified at the same time. Because the background noise from the electronic circuitry is always present as noisy baseline in the spectrum, one way to improve the accuracy and precision of the intensity measurement is to improve the S/N ratio.

One advantage of FT NMR is the ease of carrying out signal averaging. The basis

is that the signals are not random but the noise is. By collecting multiple scans for one spectrum, the signals will co-add whereas some of the noise will cancel out. In terms of the number of scans (n), the signal will be amplified by n and the noise by $\sqrt{n}$. Therefore, an overall increase of $\sqrt{n}$ in S/N can be achieved. Of course, the time factor will be a trade-off especially for large n.

Another method to enhance S/N is to modulate the envelope of the FID. Since signals decay exponentially but the amplitude of noise remains almost constant, the tail of an FID contains mainly noise. It is possible to smooth out the noise near the tail by applying a suitable apodization function.[65] An exponential function improves S/N but it also produces broad lines. A Gaussian function enhances resolution with less S/N enhancement. The choice of an appropriate function is really based on a compromise between S/N and resolution enhancement.

One prerequisite for getting good sensitivity enhancement is to have maximum observable signals. A 90° or $\pi/2$ pulse is desired since it produces maximum transverse magnetization. One potential problem is that if a signal is already strong due to high concentration or a dynamic range problem, a $\pi/2$ pulse may produce inaccurate signal intensity.

3.1.2.b Dynamic range[80-82]

NMR signals have to be converted into digital form before Fourier transformation. The resolution of the analogue-to-digital converter (ADC) and the computer memory place a practical limit on the dynamic range of a spectrum, that is, whether signal

intensities can be fully presented in a spectrum. The dynamic range of the acquired data is the range of signal amplitudes that can be detected. The dynamic range of the transformed data is the maximum scans that can be accumulated. The former is a function of the wordlength of the ADC while the latter is a function of the computer wordlength. Typical wordlength of a digitizer is 12 bits or 16 bits, characterizing a dynamic range of +/- 2048 or +/- 32768. Typical computer wordlength is 24 bits whereas in some newly-developed spectrometers it is 32 bits.

If a digitizer has a resolution of n bits, the size of a signal then ranges from 0 to 2^n-1. If one bit is used for the sign of the amplitude, the dynamic range is

$$\frac{I_s}{I_w} \leq 2^{n-1} - 1 \qquad (12)$$

where I_s and I_w are the detectable strongest and weakest signals. If the strongest signal exceeds the dynamic range, severe distortion of the signal height and phase will occur. If a weak signal is smaller than the minimum digitizable value, it will be buried under the digitization noise and never be detected unless the digitization noise is bigger than the minimum digitizable value. Baseline distortion and lower S/N are likely to be produced as well.

Next is the problem arising from the computer wordlength. After each scan, data points are accumulated and stored in the computer memory. Usually the computer wordlength is longer than the ADC wordlength to provide sufficient capacity. However, there is still possibility that the accumulation overflows the computer memory, resulting in distorted spectrum. All these, of course, impose difficulty and imprecision in

quantifying a spectrum.

3.1.2.c Saturation[78]

When pulsing a sample, the Boltzmann distribution is disturbed and the excess population in the lower energy state are excited to the upper energy state until the populations in both states are equalized. This is called saturation. The "excess" spins or the z-magnetization (M_z) returns to the lower energy state exponentially by the spin-lattice relaxation process to re-establish the Boltzmann equilibrium condition. If M_o is the equilibrium magnetization,

$$M_z = M_o\left(\frac{1-\exp(-\tau/T_1)}{1-\exp(-\tau/T_1)\cos\alpha}\right) \qquad (13)$$

where α is the flip angle of the magnetization, τ is the time interval between pulses and T_1 is the spin-lattice relaxation time constant. T_1 varies from nucleus to nucleus and it is also different for identical nuclei in different chemical environment.

When doing multiple scans experiment, the repetition rate of pulses is very important because if the pulsing is too rapid, incomplete relaxation will result and the signal intensities cannot be fully recovered. Therefore, a proper delay time between scans is crucial for quantitative NMR experiments. In order to have at least 99% signal recovery,

$$\frac{1-\exp(-\tau/T_1)}{1-\exp(-\tau/T_1)\cos\alpha} \leq 0.99 \qquad (14)$$

In most cases, a 90° flip angle is used. **(14)** is simplified to

$$1 - \exp(-\tau/T_1) \leq 0.99 \qquad \textbf{(15)}$$

and

$$\frac{\tau}{T_1} \geq 4.6 \qquad \textbf{(16)}$$

Hence, a delay time of at least 5 T_1 of the longest T_1 of the sample should be used in order to recover at least 99.3% of the signal intensity and to keep the errors from saturation below 1%.

3.1.2.d Nuclear Overhauser effect (NOE)

It is now a common practice to remove the proton coupling when doing ^{13}C NMR experiments so that only single carbon lines are observed. It is easier to extract both the qualitative and quantitative information due to the disappearance of signal multiplets. Usually noise-modulated broadband decoupling[83] is used to decouple the proton spins. However, this inevitably involves saturation of the proton spins and may cause NOE enhancement across a spectrum. The efficiency of NOE depends on the intramolecular dipolar interactions between carbons and protons which in turn depends on the internuclear distance r^{-6} and the correlation time τ_c. This implies that NOE enhancement across the spectrum may not be uniform. For instance, quaternary carbons show very small NOE because there is no attached proton and dipolar interaction is very inefficient whereas methylene and methine carbons have similar NOE. For methyl carbons,

mechanism such as spin rotation might reduce the efficiency of dipolar relaxation and hence lower the extent of NOE.

It is important to realize that the differential NOE enhancement will cause variations of the carbon intensities. Therefore, NOE must be suppressed if accurate intensity measurements are desired. One way to suppress the NOE is to use inverse gated-decoupling instead of using broadband decoupling. The key is that the NOE requires the order of T_1 to build up. If the decoupler is switched off during a relatively long waiting time and is on only during acquisition, the NOE can be effectively suppressed. Again, the importance to use at least 5 T_1 is significant.

3.2 Quantitation Methods

Having taken considerations on various parameters certainly will improve the quality of a spectrum but meaningful results also depend on how to measure the intensities and how to interpret the data. The first "how" is to be discussed in the following paragraphs whereas the analysis of data will be discussed in the next section.

3.2.1 Peak Area

Peak area measurements have been playing an important role in quantitative NMR since the recognition of the direct relationship between the NMR signals and the Boltzmann excess of nuclear spins. Another reason that this method is well-accepted by NMR people is the development of modern electronic integrators which facilitate the use

of peak area. It is a common thought in the NMR researchers' mind that integrated intensities are the most reliable representation when quantitative aspects are concerned. In terms of accuracy and precision, it is true that integrals are accurate but it is also true that they are not reproducible. Possible error sources include digital resolution, S/N ratio, integration region, phasing and baseline.

3.2.1.a Digital resolution

Routine integration is done by using the trapezoid approximation (Simpson's rule) to evaluate the integrals numerically. This requires well-defined lineshape of the integrals. The natural linewidths of proton and ^{13}C are < 0.5 Hz. The digital resolution for proton lines is typically 0.3-0.4 Hz/point whereas for carbon lines it is roughly 2-3 Hz/point. To characterize a peak properly, the linewidth of the peak must be greater than its digital resolution. Some proton lines are very sharp and have linewidth ~ 0.1 Hz. Sufficient data points must be used in order to reduce errors in the measurements. This can be done by lengthening the acquisition time, by zero-filling the FID before it is Fourier transformed or by broadening the lines with an apodization function. The first one will inevitably lower the S/N ratio while the third alternative may result in overlapping of peaks. The second alternative is used only when the tail of the FID contains no signal.

3.2.1.b S/N ratio

The presence of noise in a spectrum contributes to the random error in integral

measurements. It also creates difficulty in defining the baseline. This means that scan accumulation is necessary for getting a spectrum with high S/N ratio.

3.2.1.c Integration region

Inaccurate integral measurements can be caused by using improper integration regions. The proton spectrum of complicated molecules often show high degree of signal overlapping which raised difficulties in defining an integration region. In addition, the presence of ^{13}C satellites and spinning sidebands also causes trouble. If the peaks are well-defined, it is not a problem whether to include or exclude them as long as the choice is consistent. But if the resolution is poor, the artifacts may be buried in the overlapping peaks and may contribute to the intensity of those peaks, thus introducing errors to the integrals.

There is a simplicity when working with ^{13}C spectra due to the disappearance of multiplets and satellites and so a better resolution can be obtained. Nevertheless, the choice of integration region will still lead to erroneous area measurements since there is no definition of whereabouts to start and to end the integration.

3.2.1.d Phasing

Pure absorption mode is ideal for signal integration due to the fact that dispersion mode will reduce the signal intensity. In reality, the signals transformed from an FID usually are mixtures of absorption and dispersion modes. The spectrum thus needs to be phased-corrected before integration is performed to maintain the accuracy. Although

phasing a spectrum is a routine procedure in NMR, the quality of the appearance of the spectrum is really determined by the operator's personal preference and judgement unless iterative curve-fitting is used.

3.2.1.e Baseline

The integrals are very sensitive to small changes in the spectral baseline. Large errors can be introduced if the baseline is noisy or distorted. Even with high S/N ratio, baseline distortions can be caused by improper phase correction or by incorrect setting of the delay time for the receiver to recover from the pulsing between pulses. These are seen as baseline rolling or artifacts. Although it is very common to remove baseline distortion by applying baseline correction, however, subjective judgement will be involved.

3.2.2 Peak Height

3.2.2.a Dependence on T_2 and linewidth

The major drawback of using peak heights in analytical NMR is the dependence of the spin-spin relaxation time T_2 and the variations of the peak widths since peak heights are very sensitive to changes in linewidths. T_2 measures the decay time of the xy magnetization of a signal. Under ideal condition when the decaying process is solely by spin-spin relaxation, the linewidth or the full width at half height of a Lorenztian line is defined as

$$\nu_{1/2} = \frac{1}{\pi T_2} \qquad (17)$$

However, addition factors such as magnetic field inhomogeneity, the use of broadband decoupling, exponential apodization function or quadrupolar relaxation will cause line-broadening effect.

The static magnetic field $\mathbf{B}_o$ experienced by different part of a sample is usually not uniform. Consequently, the resonance frequency of nuclei belonged to the same group may be slightly different. This results in broadening of the transformed signal due to the spread of chemical shift. Proton-decoupled ^{13}C spectra are commonly obtained by broadband decoupling. The completeness of decoupling is determined by the decoupler efficiency, that is, whether the decoupler power is uniform across the spectrum and whether the power is strong enough to remove all proton couplings. Residual broadening of signals will be produced if the decoupler efficiency is low. It is a common practice to apply an exponential multiplication function to smooth out the noise near the tail of an FID prior to Fourier transformation (**§3.1.2**). This is done at the expense of lower resolution. The truncation of the tail corresponds to a shortening of T_2, leading to broadening of signals.

3.2.2.b T_2^* and remedies for the broadening effect

It is more realistic to use the effective transverse relaxation time T_2^* as a measure of the decaying time of the transverse magnetization. Correspondingly, the observed linewidth is

$$\nu_{1/2}^{*} = \frac{1}{\pi\, T_2^{*}}$$

$$= \frac{1}{\pi}\left(\frac{1}{T_{2nat}} + \frac{1}{T_{2inhomo}} + \frac{1}{T_{2dec}} + \frac{1}{T_{2LB}} + \frac{1}{T_{2quad}} + \frac{1}{T_{2other}}\right) \qquad (18)$$

where $\nu_{1/2}^{*}$ denotes the contribution to the broadening of lines from the natural relaxation process and other line-broadening factors.

It is important to know how these factors affect the linewidth of the proton, carbon and deuterium signals. For most protons, T_2 is about 1 sec so $1/T_{2nat} < 0.5$ Hz. With modern high-resolution spectrometers, the effect of field inhomogeneity can be scaled down to 0.5 Hz by good shimming. Obviously, no decoupling term is involved with proton spectra. Thus, if a heavy line-broadening (LB) factor is applied, the observed linewidths of the proton lines will be dominated by the LB factor. Since carbon lines are less dependent on field inhomogeneity, $1/T_{2inhomo}$ is negligible. The two determining factors are actually the decoupler efficiency and the operating LB value. Although broadening by decoupling may be as large as 3-5 Hz, decouplers are stable enough to maintain same broadening effect throughout the whole ^{13}C spectrum. The only dominating factor is again the LB factor if it is comparably large. In the case of quadrupolar nuclei such as deuterium, quadrupolar relaxation very often dominates the dephasing of the xy magnetization and cause significant line-broadening.

The preceding discussion is not intended to discourage the use of integrals. It is to show that peak heights can be as useful as integrals. In comparison to integrals, peak heights vary very little with small changes in phasing while integration region needs not

be considered. In terms of dependence on resolution, peak heights are less affected by peak overlapping. Similar to integration, measurements with peak heights are also affected by the S/N ratio and baseline problems, however, to a less extent. The information of interest is the relative peak heights rather than the absolute values. In terms of precision and accuracy, the associate precision will not be affected by errors due to low S/N ratio or poor baseline if these errors are of a constant value, and the accuracy can be recovered by calibration methods.

Instrumental errors are correctable or at least they are systematic. On the contrary, errors caused by improper choice of integration region, improper phase correction and baseline correction are of personal bias and they are unavoidable and random. Examine the factors affecting both methods again, peak height measurements can be carried out if same amount of consideration and carefulness have been taken.

3.3 Data Analysis

Quantitation by the peak height method relies largely on proper handling of data since the accuracy and precision of the method will be affected. All numerical analyses in this thesis start with the relative peak heights.

When a calibration method is used, the most valuable information is the slope of the calibration curve. Relative peak heights are advantageous in the way that if any constant errors are present, the slope will not be affected. The two methods used to obtain the relative peak heights are external and internal referencing methods. The

advantages have been discussed in some papers.[84-86,58] In external referencing method, a substance (solvent in most cases) separately contained in either an NMR tube or a concentric tube is used as an external reference. Signal heights are made relative to this reference. In internal referencing method, one of the intramolecular peaks is used as an internal reference.

Accuracy and precision are two terms that determine whether an analytical method is reliable. Chemometrical methods can be applied.[87,88] If the peak height method works, there will be a linear relationship between the relative peak heights and the concentration of the observed nucleus. To validate the method, a linear model is needed to test the correlation between the two variables. This is done by using calibration with the relative peak heights and the mole fraction of the sample as the respective dependent and independent variables. It would be helpful to have a cross-check with the results obtained by this method. This is done by having an "unknown" with known concentration. Having an internal cross-check provides a means to compare the accuracy of the experimental results.

The calibration can be checked by applying statistical analysis to the data derived from block averaging. Instead of collecting many scans for one spectrum, block collection is used in which the total number of scans is broken down into blocks of scans. In this way, the S/N ratio is preserved since the total number of scans is still the same as before, but average and standard deviation can be obtained for further statistical analysis such as F-test, weighted-least-squares analysis and the analysis of variance (ANOVA). Errors may be random or systematic. An advantage of using block averaging

is that for no cost in acquisition time it becomes possible to recognise and distinguish the random and systematic errors. Assuming that errors are indeed random, the precision of the data can be improved by using more blocks.

Block averaging begins with a series (block) of spectra which are acquired under identical conditions and processed with identical parameters. Given sets of peak heights measured from individual spectra in the same block, two approaches can be used to calculate the average and standard deviation (SD) of a relative peak height. The first approach calculates the ratio of averages (RoA) while the second one looks for the average of ratios (AoR). If a block contains 10 spectra and each spectrum contains one signal peak and one reference peak, there will be a total of 10 similar peak heights for the signal and reference peaks in the block. In the first approach, an average value and the associate standard deviation of the 10 peak heights is first obtained for both the signal and reference. The relative peak height is then obtained by taking the ratio of the average signal height to the average reference height. The respective standard deviation is related by combining the standard deviations associated with both peak heights. Experimentally, raw peak heights can be obtained by using the peak-picking routine designed for processing NMR data or by using a program NMRSTAT, written in Pascal, to perform block averaging. If NMRSTAT is used, an average and a SD spectra will be produced (**Figure 6**). Raw peak heights obtained by peak-picking are processed by spreadsheet programs. In the second approach, the ratio of each signal-reference pair in each spectrum is first calculated. The average is then computed by averaging the 10 ratios. The SD is simply the SD of the 10 ratios.

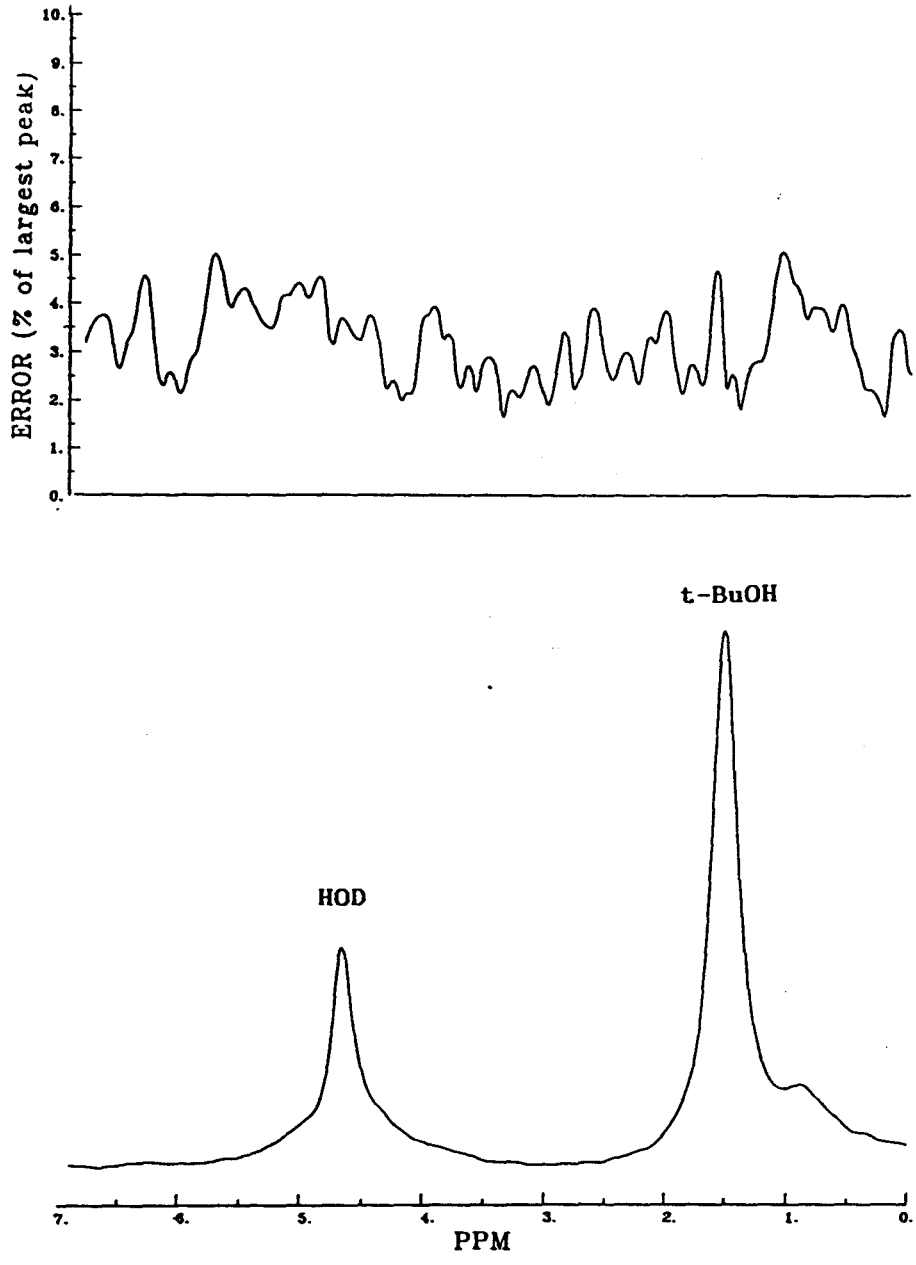

Figure 6. Average and standard deviation spectra of water and t-BuOH obtained from NMRSTAT. The water peak is located downfield.

Without the aid of computers and computer programs, data analysis would be very time-consuming or less accurate. The improvement of microcomputers in FT-NMR spectrometers and the use of automation procedures[41] enable sophisticated data analysis to be performed in a reasonably short period. It is now possible to transfer data from a spectrometer to a stand-alone computer where data can be processed and analyzed with NMR and spreadsheet packages.

To conclude this section briefly, the various ways of statistical analysis will not produce more accurate peak height values. They are used to give an honest reflection on the quality of the acquired data.

3.4 Consideration of the NMR Experiments

The emphasis so far is getting quantitative NMR spectra. In other words, unwanted spectral effects such as saturation of signals, spin population transfer through dipolar relaxation and incomparable signal strength must be avoided. This was achieved by adjusting the experimental conditions in preparing samples, acquiring and processing NMR spectra. The following is a list of steps that were considered in running the NMR experiments. These steps were actually developed from the experiments and some of them will be discussed in later sections.

1. Samples were gravimetrically prepared.
2. Approximately 5-7 mM of relaxation reagent, $MnCl_2 \cdot 4H_2O$ or $Cr(acac)_3$, was added to sucrose and sucrose octaacetate (SOAc) to shorten the T_1 of carbons.

3. The choice of solvent was considered to avoid solubility, viscosity and dynamic range problems.
4. Concentric (coaxial) tube was used in some experiments to separate the sample from the referencing material and to produce comparable signal intensities.
5. Bruker AMX 500, AM 500, WM 250 or AC 200 NMR spectrometer was used.
6. Temperature of the probe was fixed at 303 K or 30°C.
7. Quadrature detection was used for all NMR experiments.
8. Deuterated solvents were used to provide the lock signal.
9. Spinning was often off to eliminate spinning sidebands.
10. The pulse width of the observed nucleus was calibrated prior to acquisition.
11. A 90° flip angle was used to give maximum signal intensity.
12. T_1 of the nucleus of interest was measured by the inversion-recovery sequence.
13. Automated procedure was employed. A simple [5 T_1 - $\pi/2$ - acquisition] sequence in which the decoupler was gated off during the delay time was used to acquire the FIDs.
14. The spectral width was wide enough to include all signals.
15. Block averaging was used so to recognise any random or systematic variations.
16. Optimal decoupler power was applied to improve the line-shape.
17. Sufficient data points were used to produce well-defined lines.
18. Zero-filling was occasionally used to improve digital resolution.
19. Exponential apodization function was applied to weight the FIDs so to smooth out the noise as well as to broaden the lines.

CHAPTER 4 QUANTITATIVE ^2H EXPERIMENTS

4.1 Introduction

The standard method for the determination of deuterium (^2H) in water has traditionally been isotope-ratio mass spectrometry.[89,90] This requires a somewhat specialised mass spectrometer in which water is reduced to hydrogen so that the HD^+/H_2^+ or the D/H ratio can be measured. For this reason, any water mixture undergoing mass-spectrometric analysis must have water separated from the mixture before entering the spectrometer. This is essential not only to avoid interferences in the mass spectrometric analysis, but also to avoid contamination of the uranium catalyst used to crack the water. This is especially true for mixtures containing DMSO. Moreover, excellent resolution is needed to distinguish HD^+ from the common ion H^{3+}. Mass spectrometry is the most sensitive method but drawbacks such as presence of interferences and memory effects, in addition to those mentioned in Chapter 1, has aroused people's interest in using NMR.

The first attempt to quantify the deuterium content in natural waters with ^2H NMR was carried out a decade ago.[91] Recent work is mostly done by Martin *et al.*[92-102] The experimental interest in this part is the concentration of deuterium (^2H) in deuterium-enriched or -depleted water samples and DMSO/water mixtures. Since deuterium is quadrupolar, signal width is dominated by the broadening of quadrupolar relaxation. The

peak height method is therefore deliberately used.

The work involved validation of the quantitation method by using relative peak heights as well as application of the method to the analysis of DMSO/water mixtures. The reliability of the method was tested by analyzing the data statistically. Pure water experiments were performed to validate the method. The procedure included constructing calibration curves with standard waters whose deuterium concentrations were known, and testing the calibration curve with a standard water. Next, the method was applied to a DMSO/water mixture having unknown deuterium content. The amount of deuterium was found by spiking the mixture with a standard water. Either t-BuOH or DMSO was chosen to be the reference peak in the pure water experiments for they showed up as a single peak in the deuterium spectrum and did not interfere with the HOD peak. Since the reference was separately contained in a concentric tube or an outer NMR tube, it was used for the whole series of samples during the experiment. In the DMSO/water experiment, DMSO was used as an internal reference, taking the advantage of the fact that it was already present in the sample.

4.2 Method

In principle, if the relative peak heights are proportional to the total number of deuterons present in the waters, the calibration plot should be linear when the relative peak heights are plotted against the mole fraction of one of the standard waters. The deviation of the slope estimates the quality of the line. If R_D is the relative deuterium

signal and X_f the mole fraction, then

$$R_D = a + b X_f \tag{19}$$

where a and b are the respective intercept and slope.

The second step is to use the above model to find out the deuterium concentration in a DMSO/water mixture. If the amount of DMSO in the mixture is known, information can be extracted solely from the deuterium spectra by spiking the mixture with a standard water. If the amount of DMSO is not known, proton spectra are used to provide the knowledge of the mole fraction of DMSO. By employing both ^1H and ^2H NMR, relative or absolute deuterium enrichment or depletion can be found.

Mathematically, if

y = mole fraction of DMSO in DMSO/water mixture

X_m = moles of DMSO/water mixture

X_s = moles of standard water

α,β,γ = deuterium concentration in different waters

K = proportionality constant which incorporates stoichiometric constant and constant relating peak heights to the number of nuclei

R_D = relative peak height of HOD peak to DMSO peak

then

$$R_D \propto \frac{Total\ number\ of\ deuterons\ of\ water}{Total\ number\ of\ deuterons\ of\ DMSO} \tag{20}$$

$$R_D \propto \frac{Deuterons\ (\ standard\ water\ +\ water\ of\ mixture\ )}{Total\ deuterons\ of\ DMSO}$$

$$R_D = K\,\frac{\alpha X_s + \beta\,(1 - y)\,X_m}{\gamma\, y\, X_m}$$

$$R_D = \frac{K\,\beta}{\gamma\, y}\,(1 - y) + \frac{K\,\alpha}{\gamma\, y}\,\frac{X_x}{X_m} \qquad (21)$$

It is clear that the relative peak height, R_D, is linearly related to the mole ratio of standard water to the mixture. Taking the quotient of the intercept (I_D) to the slope (S_D)

$$\frac{I_D}{S_D} = \frac{\beta}{\alpha}\,(1 - y) \qquad (22)$$

(22) indicates that if the mole fraction, y, is known, then the relative deuterium enrichment (β/α) or the absolute amount of deuterium (β) in the mixture can be found provided that α is known. The mole fraction of DMSO in the sample can be measured in a number of ways, such as refractometry, but since a proton NMR spectrum can be easily acquired this information can be obtained by NMR. For a mixture with unknown mole fraction of DMSO, proton spectra give the following:

$$R_H = K\frac{X_s + (1-y)X_m}{yX_m}$$

$$R_H = \frac{K}{y}(1-y) + \frac{K}{y}\frac{X_s}{X_m} \qquad (23)$$

where R_H is the relative peak height of the H_2O peak to the DMSO peak. For a plot of R_H against X_s/X_m, the quotient of the intercept (I_H) to the slope (S_H) is

$$\frac{I_H}{S_H} = 1 - y \qquad (24)$$

Hence, y can be recovered.

4.3 Experimental

4.3.1 Validation

Water samples containing 9.5, 52.6, 148 and 493 ppm deuterium (ppmD), measured by mass spectrometry and supplied by Ontario Hydro, were used in two mixing experiments. The references, t-BuOH and DMSO, were standard laboratory material. Two of the waters, 148 and 493 or 9.5 and 148, were mixed to give samples with varying mole fraction for constructing the calibration plots. t-BuOH was used as an external reference in the former mixing experiment. In the latter case, DMSO was used and 52.6 ppmD water was treated as an unknown to check the reliability of the calibration method.

The deuterium spectra were acquired on the Bruker WM 250 MHz FT NMR

spectrometer equipped with a 10-mm VSP broadband probe at ambient temperature without field-frequency locking. The operating frequency was 38.4 MHz. 10-mm NMR tubes (Wilmad 513-1PP) together with a concentric tube (Wilmad WGS-10BL) were used. When t-BuOH was used as the reference, it was put in the outer 10-mm tube whereas when DMSO was used, it was put in the concentric tube. In this way, the strength of the water signal and the reference were comparable. The precautions mentioned before were observed. The T_1 of t-BuOH and DMSO were measured by the inversion-recovery sequence and they were 0.14 and 0.56 sec respectively (**Table 1**). A recycle time of 3 sec was used to ensure full recovery of signals. A 90° pulse width of 37 μs was used. The spectral width was 800 Hz and the digital resolution was 0.4 Hz/pt. Exponential apodization with a broadening factor of 5 Hz was applied. A total of 1200 to 9600 scans were collected in 10 blocks, depending on the deuterium concentration in the water samples.

4.3.2 DMSO/Water Experiment

A DMSO/water solution containing 0.464 mole fraction of DMSO was made up with 9.5 ppmD water. The solution was then diluted with the addition of 52.6 ppmD water to make up a series of mixtures with varying mole ratio of the 52.6 ppmD water. In this experiment, the 9.5 ppmD water was treated as the unknown and the 52.6 ppmD water served as the standard. The ^2H NMR parameters were similar to those in the two mixing experiments except that the spectral width was 1000 Hz, giving a digital resolution of 0.5 Hz/pt, and that the number of scans was 2400 in 10 blocks.

The proton spectrum of each mixture was acquired on a Bruker AC 200 MHz FT spectrometer. Sample solutions were put in a concentric tube (Wilmad WGS-5BL) and $CDCl_3$ was put in the outer 5-mm NMR tube (Wilmad 507-PP) to give the lock signal. Since the proton T_1 of DMSO was found to be 2.54 sec (**Table 1**), a total delay time of 15 sec was used. The pulse width was 1 μs (12.4° flip angle) and 128 scans were collected for each spectrum. The resulting lines were 0.3 Hz wide and a 5 Hz line-broadening factor was applied.

Raw data were processed either on the Aspect 3000 attached to the spectrometer or were shipped over to a stand-alone computer and processed by an NMR package called NMR286. The average and standard deviation of the relative peak heights were calculated by the methods introduced in **§3.3**. The rest of the statistical analyses were done by spreadsheet software.

Table 1. Proton chemical shift and T_1 value of some solvents

Solvent	Chemical Shift (δ)*	T_1 (sec)
Acetone	2.04	4.79
tert-Butanol (t-BuOH)	1.06 (TSP)	0.14
Cyclohexane	1.38	1.83
Deuterium oxide (D_2O)	4.67 (TSP)	0.55
Dimethyl sulphoxide (DMSO)	2.49	0.56
Hexamethyl disiloxane (HMDSO)	0.27	1.41
N-Tetramethyl urea (TMU)	1.84	1.08

* $\delta_{reference}$ is TMS except when otherwise specified.

4.4 Results and Discussion

Three things must be considered when choosing an external or internal reference: the chemical shift, T_1 and the strength of the deuterium signal. The deuterium chemical shift of HOD is 4.67 ppm (**Table 1**). The reference is best 2 ppm away from the HOD signal to avoid any overlapping. The fact that 5 T_1 is needed between scans suggests that short T_1 is preferred so that higher S/N can be achieved at a reasonable experimental time. Since the relative peak heights are used, better precision can be obtained if the signal strength of the reference and the HOD peak is comparable. Comparable strength also avoids running into dynamic range problems (**§3.1.2.b**). Several organic solvents had been examined in this experiment. Their chemical shifts and T_1 values are listed in **Table 1**. Acetone had been used as a reference[91] but a recycle time of 24 sec would be too time-consuming if there exists a better choice. It is obvious that t-BuOH and DMSO would be the choice since they have shortest T_1 values. Experiments showed that their signal strength was tolerable.

It is worthwhile to point out that the OH on t-BuOH might have small contribution to the signal of the water peak in the first water mixing experiment. The contribution would be constant to all spectra since the same t-BuOH in the outer 10-mm tube was used throughout the experiment. This would certainly cause erroneous measurement if absolute peak heights were used. With relative peak heights, this constant would only affect the intercept (shifting the whole calibration curve upward) without causing any changes to the slope of the line. Since what is important in a calibration plot

is the slope of the curve, the accuracy of the result would not be affected.

Table 2 is an ANOVA table which summarizes the result of variance analysis for the first pure water mixing experiment, mixing of 148 and 493 ppmD waters. At 95 % confidence limit (C.L.), almost all the points lie within the error bars, but they failed the F-test for linearity at this confidence limit (F_{expt} = 5.55, $F_{0.5,3,45}$ = ~3.4). **Figure 7** is the calibration plot obtained by mixing 9.5 and 148 ppmD waters. The line is not straight statistically at 95 % C.L. but the unknown (52.6 ppmD) is right on the regression line.

Table 2. ANOVA table summarizing the results of pure water experiment of 148 and 493 ppmD

Source of Variation	Sum of Squares	Degrees of Freedom	Mean Square
Due to regression	SS_{reg} = 0.007	1	
Lack of fit	SS_{lof} = 2.664	3	8.69×10^{-4}
Pure error	SS_{pe} = 0.003	45	1.57×10^{-4}
Total	SS_t = 2.654	49	

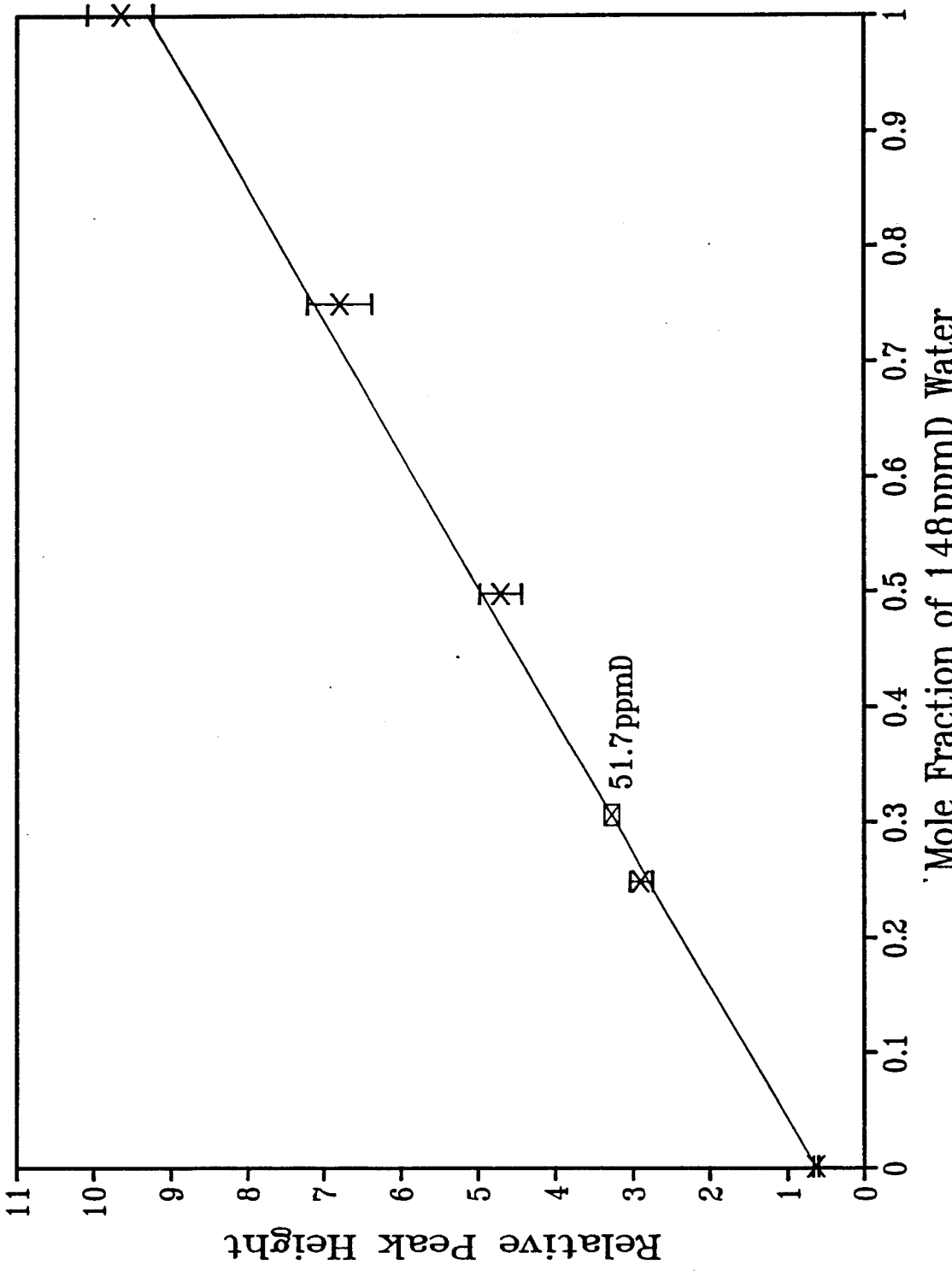

Figure 7. Calibration plot of 9.5/148 ppmD water mixture. The observed value for the "unknown water" (52.6 ppmD) is 51.7 ppmD.

Assuming errors are random, the linearity of a calibration plot is evident by the fit of the line within the error bars. The observed deviation of the two calibration curves might be a sign of the presence of small systematic errors, possibly due to instrumental instability. It might also be an indication of the precision limit of the method. If errors were truly random, the S/N ratio or the standard deviation of the slope would be improved with the use of block averaging. The 2-3 % error level found in these pure water mixing experiments might signify that the improvement had reached its limit. It was found in a later experiment that the standard deviation of the signal heights showed dependence on the flip angle of the pulse. Moreover, any instability in the amplifier would also introduce a determinate error. The calibration curves would be linear if a wider confidence interval had been used. At a 2-3 % level, the calibration method is considered acceptable.

The two approaches taken to calculate the average and standard deviation (SD) of the relative peak heights resulted in different SD values. It was found that the average of the ratios produced smaller standard deviations. The idea has already been introduced in §3.3. It is further explained by that spectra in the same block did not have identical signal intensities due to the electronic fluctuations. When the average peak height of the water peak and the reference peak in each block was calculated, the scattering of peak heights determined the magnitude of the precision. When the ratio of each pair was first computed, the errors were also ratioed out and consequently smaller SD were obtained.

The DMSO/water experiment revealed the applicability of the method. Since the mixture was simulated, internal check on the results was possible. The presence of

DMSO in the mixture provided a good internal reference. Although chemical exchange between water and DMSO easily occurs at basic pH, no exchange was observed under the experimental conditions, *i.e.*, neutral pH.

Equation **(22)** indicates that the mole fraction of DMSO in the mixture is crucial for finding the deuterium concentration. The mole fraction is usually determined by measuring the refractive index of the mixture. In this experiment, this was done by using ^{1}H NMR. The proton and deuterium lines obtained by spiking the mixture with 52.6 ppmD water are shown in **Figure 8**. By using **(24)**, the mole fraction, y, was found to be 0.4649 +/- 0.0208 which well agreed with the simulated y value of 0.4643. For the purpose of comparison, integrals of the proton peaks were also measured and a y value of 0.4522 +/- 0.0204 was obtained. It is clear that peak heights gave more accurate y value in this instance.

It is seen in **Figure 8** that the relative errors in the first two points of the deuterium line are large but the absolute errors are comparable. Consider that the water used to make up the mixture was only 9.5 ppmD, which is very dilute if comparing with the natural abundance of deuterium in ordinary water. The first two points correspond to 9.5 ppmD and the first spike with 52.6 ppmD water. The corresponding deuterium signals are relatively weak and this is why large uncertainties were found in measuring these two points.

Table 3 summarizes the slope, intercept and the deuterium concentration of the DMSO mixture found experimentally. The deuterium content (β) was found to be 7.3 +/- 3.2 ppmD. At first glance, the relative standard deviation of β (43.7 %) might be too

high for proving that the method works. However, two things should be considered. Firstly, the major contribution to the error of β comes from the intercept of the deuterium line, as shown in **Table 3**. This has been explained in the previous paragraph. The magnitude of this error would be smaller if more concentrated deuterium water had been used. Secondly, the absolute standard deviation is 3.2 ppm which when compared with water sample having ordinary deuterium concentration,[103,104] is of 2 % relative error. This is acceptable in terms of analytical precision. If 9.5 is taken as the true value, the t-value was found to be 1.544. Comparing with t_{crit} which is 2.776 at 95 % C.L., the result is accepted by the t-test. This implies that no significant systematic errors were present and the result is reliable at this confidence limit.

In summary, the suggested model was validated by the linear relationship between the relative peak heights and the mole fraction found experimentally. The application of the method to DMSO/water mixtures also resulted in good accuracy and precision.

Table 3. Experimental results of DMSO/water experiment

	$I_{x=0}$*	I_{cal}#	Slope#	β_{cal}†	β_{true}‡
Value	0.042	0.023	0.307	7.3	9.5
SD	0.014	0.010	0.008	3.2	

* $I_{x=0}$ corresponds to the relative peak height of DMSO/water mixture with no spike
\# I_{cal} and Slope are intercept and slope calculated by weighted-least-squares regression
† β_{cal} is the calculated deuterium content in the mixture
‡ β_{true} is the given deuterium content.

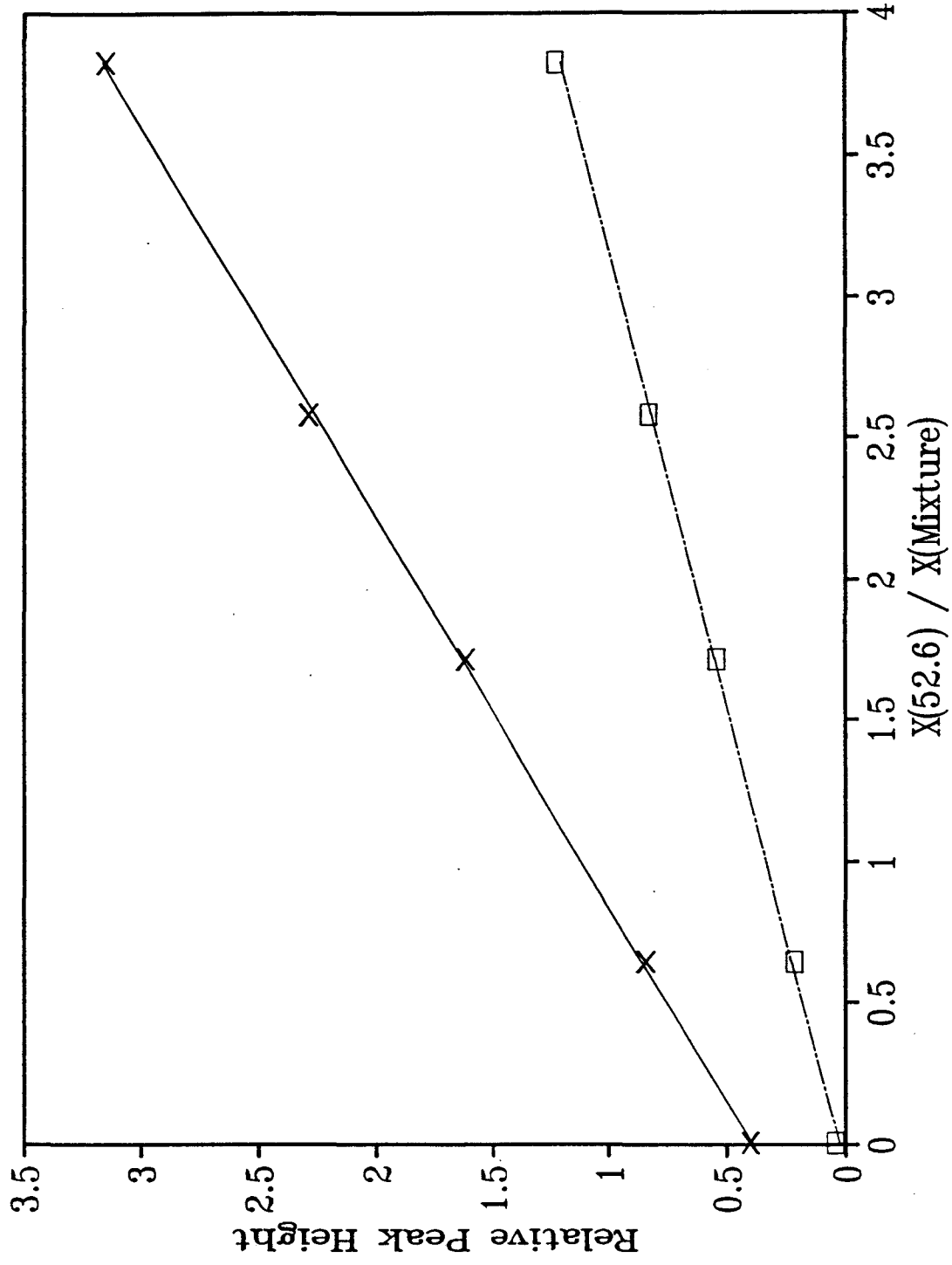

Figure 8. Plot of the relative deuterium and proton peak heights of water *vs.* the mole fraction of standard water (52.6 ppmD) to DMSO/9.5 ppmD water mixture.

CHAPTER 5 QUANTITATIVE ^{13}C EXPERIMENTS

5.1 Introduction

The objective so far is to see how effective NMR can be as a quantitative technique. In particular, the feasibility of the peak height method is critically studied. It has been demonstrated in Chapter 4 how the method works for quantitative ^{2}H NMR. It is in this chapter that quantitative ^{13}C NMR for small molecules is being studied.

The biosynthesis of sucrose in sugar cane (C_4 plant) and sugar beet (C_3 plant) involves indistinguishable enzymatic mechanisms.[105-107] However, the photosynthetic routes of CO_2 fixation in these plants are different. Cane sugar is synthesized via C_4 (Hatch-Slack cycle) photosynthetic pathway whereas beet sugar is synthesized through C_3 (Benson-Calvin) cycle. This results in a different degree of discrimination against the carbon isotope ^{13}C. The degree of discrimination or isotope enrichment is described by the isotope fractionation ($\delta^{13}C$) expressed in ‰ and is determined by mass spectrometric methods. The δ value differs slightly from species to species for the same photosynthetic group. It has been found that cane sugar has higher ^{13}C enrichment than beet sugar. An estimate of the ^{13}C difference between the two types of sugars is ~ 2-30 ‰ or 0.2-3 %.[108,109]

Although mass spectrometry provides the overall ^{13}C enrichment in cane and beet

sugars, the enrichment at individual sites cannot be measured. On the other hand, an NMR spectrum provides not only the isotope difference but also the location where this difference is found. The objective of this part of the thesis is that by analyzing the ^{13}C spectra of sucrose synthesized from sugar cane and sugar beet, the site-specific ^{13}C difference may be obtained.

The use and advantages of referencing method has been introduced in §3.3. For sucrose experiments, both external and internal referencing methods are used. A solvent is taken as the external reference or one of the ^{13}C signals is taken as the internal reference. The structure of sucrose and the numbering scheme can be found in **Figure 9a**. Although it is the carbon skeleton which is of interest, the internal reference method stated above does not tell whether a particular site is being enriched or depleted. This information should be able to be obtained by the external method in theory but in practice difficulties arise. These will be discussed later. It is practical to think of using a sucrose derivative as an internal reference. The acetate methyl group in sucrose octaacetate is thought to serve this purpose. The structure of sucrose octaacetate is depicted in **Figure 9b**.

The experiments consisted of running ^{13}C spectra of sucrose and sucrose octaacetate. Pure cane/beet as well as mixing experiments were performed. Various experimental designs were established to find out the optimal conditions for the peak height measurements. In particular, the effect of solvent, spinning of samples, recycle time, decoupler power, apodization function and machine stability on the reproducibility of spectra were experimentally observed. However, it should be noted that considerations

listed in §3.4 were observed in general. The precision of the method was found by carrying out statistical analysis on data.

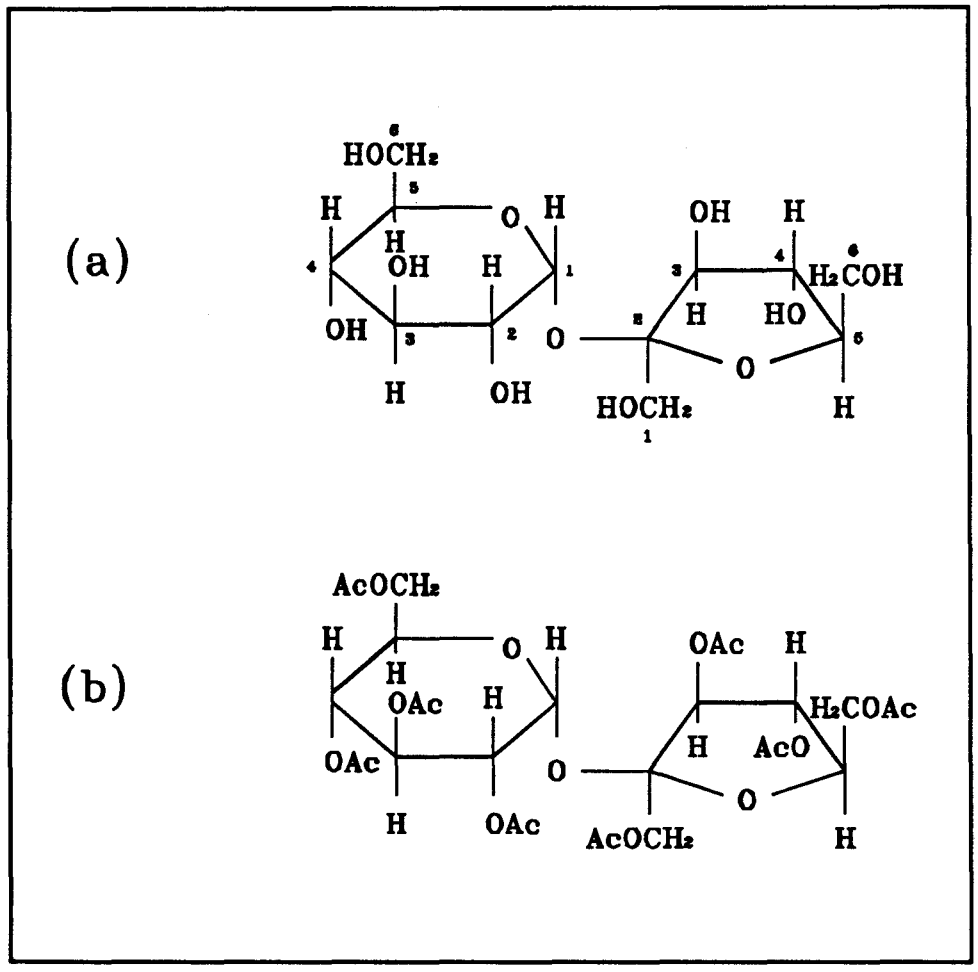

Figure 9. Structure of (a) sucrose and (b) sucrose octaacetate. The numbering scheme for the sucrose carbons are shown in (a).

5.2 Experimental

5.2.1 Sugar Experiment

The sugar experiments consisted of pure sugar and mixing experiments. Redpath cane and Alberta beet sugar were used to prepare the sugar solutions. For mixing experiments, a series of mixing solutions having varying mole fraction of cane/beet were prepared. 5-7 mM of the relaxation reagent, $MnCl_2 \cdot 4H_2O$, was added to each sample. At this concentration, the spin-lattice relaxation can be enhanced efficiently without causing too much line-broadening. D_2O was added to provide the lock signal. The final concentration of the samples ranged from 0.6-0.65 M but it was kept consistent for samples within the same experiment. A 4-M acetonitrile (CH_3CN) was also prepared to be the external reference.

Two mixing experiments were performed. The first one was run on the Bruker AM 500 MHz FT spectrometer at an operating frequency of 125.8 MHz. Solutions were put in 10-mm NMR tubes while the external reference, acetonitrile, was put in a concentric tube. A total of 6000 scans in 10 blocks were acquired. The T_1 of methyl-C in CH_3CN was measured to be 1.06 sec and the T_1s of sucrose were < 0.4 sec so a recycle time of 6 sec was put between scans. A 90° pulse width (PW) of 13.5 μs was used. The size (SI) of the FIDs was 64K. Decoupler power (DP) was 10H and spectral width (SW) was 17857 Hz.

The second mixing experiment was done on the Bruker AMX 500 MHz FT spectrometer at an operating frequency of 125.8 MHz. 3200 scans in 10 blocks were

collected with a delay time of 10 sec. SI of the FIDs was 32K, SW 15625 Hz and DP 10H.

The spectra of pure cane and beet were acquired on a Bruker AC 200 MHz and on the AMX 500 MHz spectrometers. No reference was used. The NMR parameters for the ones done on the AC 200 were: operating frequency 50.3 MHz, SW 13158 Hz, SI 16K, DP 22H, 90° PW 5.5 μs, recycle time of 6 sec and a total of 22400 scans in 10 blocks. Also, samples were put in 5-mm NMR tubes. The parameters for the ones done on the AMX 500 were identical to those for the mixing experiment done on the same spectrometer.

5.2.2 Sucrose Octaacetate Experiment

5.2.2.a Synthesis of sucrose octaacetate

Material: sucrose (BDH, analytical grade)
Redpath cane sugar
Alberta beet sugar
anhydrous sodium acetate (Caledon Cat.7120-1)
acetic anhydride
95 % ethanol

The procedure of the synthesis followed Experiment 1 in Ref. 110 except that the synthesis was done on a smaller scale. Preheated sucrose and distilled acetic anhydride were used. A mixture of 5 g of sucrose, 3.3 g of anhydrous sodium acetate and 31 mL of acetic acid was heated on a steam-bath for 25 hours. the amber product obtained was

poured on a 500-mL beaker of ice-water and left in the refrigerator for one day. The yellowish white solid obtained was filtered, washed with ice-water and roughly dried in air. It was dissolved in 24 mL of 95 % ethanol (charcoal) and the solution obtained was then filtered, crystallized at room temperature. When needle-shaped crystals had grown, the solution was put in the refrigerator for complete crystallization. The product was then filtered, washed with small amount of cold ethanol and vacuum-dried. Phosphorus pentoxide was used as the drying agent. A yield of 60 mole % was obtained, the mp was 80.5-81.56 °C.

Similar procedure was used to synthesize cane and beet octaacetate. 30 g of each sugar was used to start with. Modification was made on the heating apparatus. Instead of using steam-bath, an oil-bath with temperature fixed at ~107 °C was used. Also, the mixture was magnetically-stirred while being heated. A mp range of 75-81 °C was obtained. The product yield after first crystallization was 74-75 mole %. The purity of the product was checked by thin-layer chromatography (TLC) and proton-decoupled ^{13}C NMR.

5.2.2.b Preparation of samples

0.8 M of cane and beet octaacetate solutions were prepared in deuterated benzene (C_6D_6). Small amount of $Cr(acac)_3$ was added to obtain a concentration of 5-7 mM of Cr^{3+}. Various amount of cane and beet octaacetate were mixed to give 5 solutions having about 0, 0.25, 0.5, 0.75 and 1 mole fraction of cane octaacetate. Deuterated benzene served as the external reference.

Spectra were run on the AM 500. Samples were put in 10-mm NMR tubes. The T_1 of benzene was measured to be 1.16 sec so 7 sec was put between pulses. The NMR parameters are listed in **Table 4.**

Some of the instrumental and NMR parameters were checked for optimal conditions, using the same beet octaacetate sample from the mixing experiment. They were spectrometer of different field, spinning, recycle time and decoupler power (**Table 4**). The effect of solvent signal on the spectral appearance was examined by acquiring sucrose octaacetate in solvents such as deuterated chloroform, methanol, acetonitrile and acetone on the AC 200. For these spectra, a delay of 10 sec was put between pulses. A 90° PW of 5.5 μs was used.

Table 4. Experimental conditions for sugar octaacetate mixing experiment and for pure beet octaacetate experiment.

	Mixing Experiment	Beet Octaacetate		
Field (MHz)	500	250		
Operating frequency (MHz)	125.7	62.9		
SW (Hz)	25000	15151		
PW (μs)	11.2	37.0		
α (°)	90	90		
SI	32K	16K		
Resolution (Hz/Pt)	1.526	1.850		
DP	10H	5H	3H	3H
NS	480	512	256	256
Blocks	10	10	10	20
Spinning	on	off	off	off
D1 (sec)	7	10	20	60

Abbreviation: SW - spectral width
PW - pulse width
SI - size of an FID or number of datapoints
DP - decoupler power
NS - number of scans
D1 - recyle time or delay time.

5.3 Results and Discussion

The spectrum of sucrose, sucrose octaacetate in benzene-d6 and the spectrum of sucrose with CH_3CN as the external standard are shown in **Figures 10, 11** and **12** respectively. The % ^{13}C difference of different carbon sites of cane and beet sugars are shown in **Tables 5, 6** and **7**. They were calculated with respect to different references: C1 of glucose unit in sucrose (**Table 5**), C5 in fructose unit (**Table 6**), methyl-C of CH_3CN and acetate methyl of sucrose octaacetate (**Table 7**). The labelling scheme of sucrose can be found in **Figure 9a**. The % standard deviation (%SD) obtained from various measurements are tabulated in **Tables 8** and **9** in which the results are the %SD of the average of ratios (AoR) and the ratio of averages (RoA). These %SD are standard deviations associated with peak heights relative to G1. Similar pattern was observed when F5 was used to be the reference peak. Some of the carbon lines are drawn in **Figures 14** and **15**, showing the correlation of the relative peak heights to the mole fraction of sucrose or sucrose octaacetate. In the following paragraphs, some spectral features observed experimentally are to be discussed first before getting into the discussion of the numbers so that the effect of some experimental parameters on the final precision will be exemplified.

In the octaacetate mixing experiment, artifacts and drifting phase were observed in the resulting spectra. The FIDs were acquired while samples were spun and therefore the artifacts were suspected to be spinning sidebands. Theoretically, spinning of sample helps to remove field inhomogeneity so to reduce line-broadening. The trade-off is that

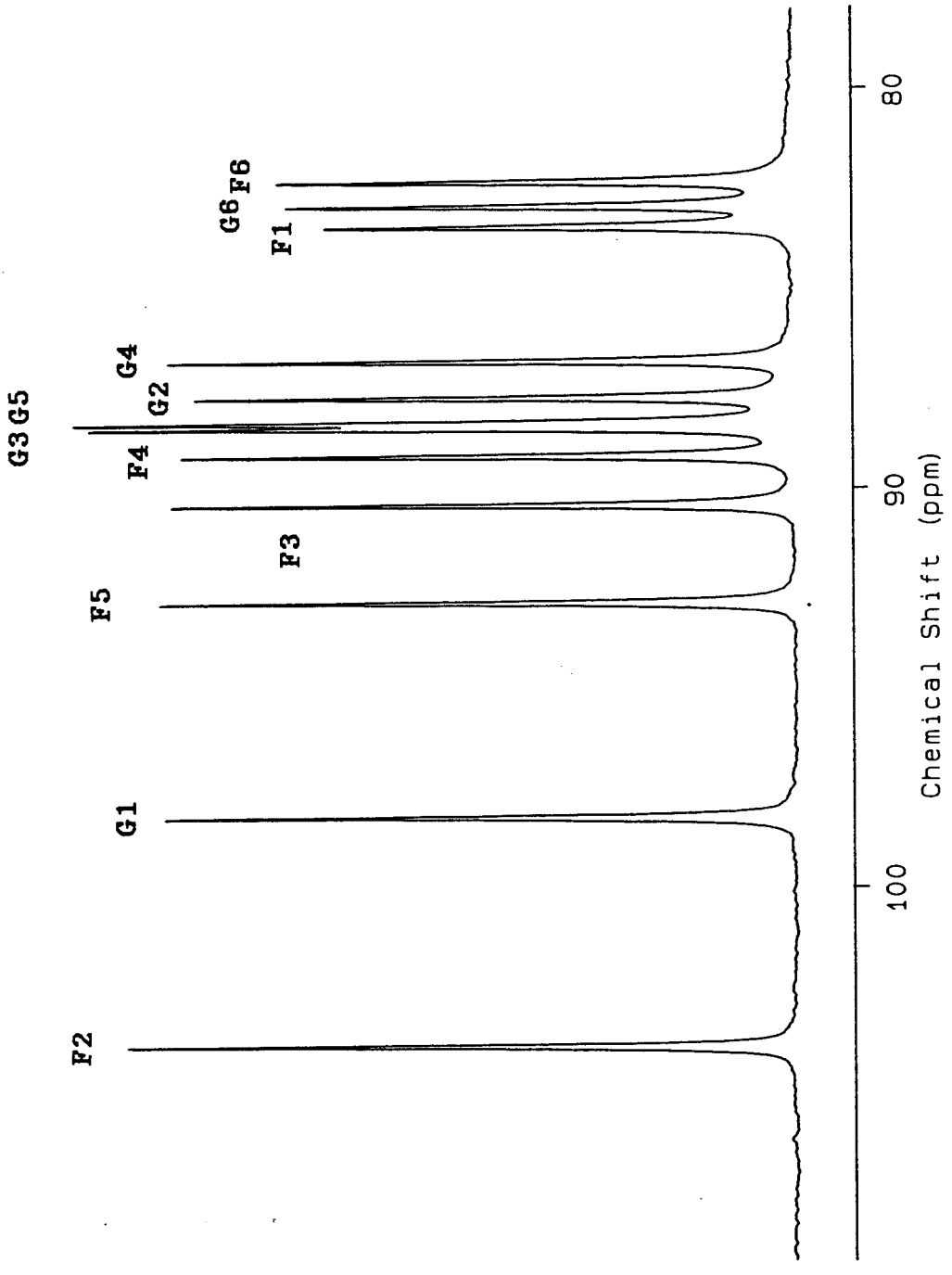

Figure 10. Spectrum of sucrose acquired on the Bruker AMX 500 MHz FT spectrometer.

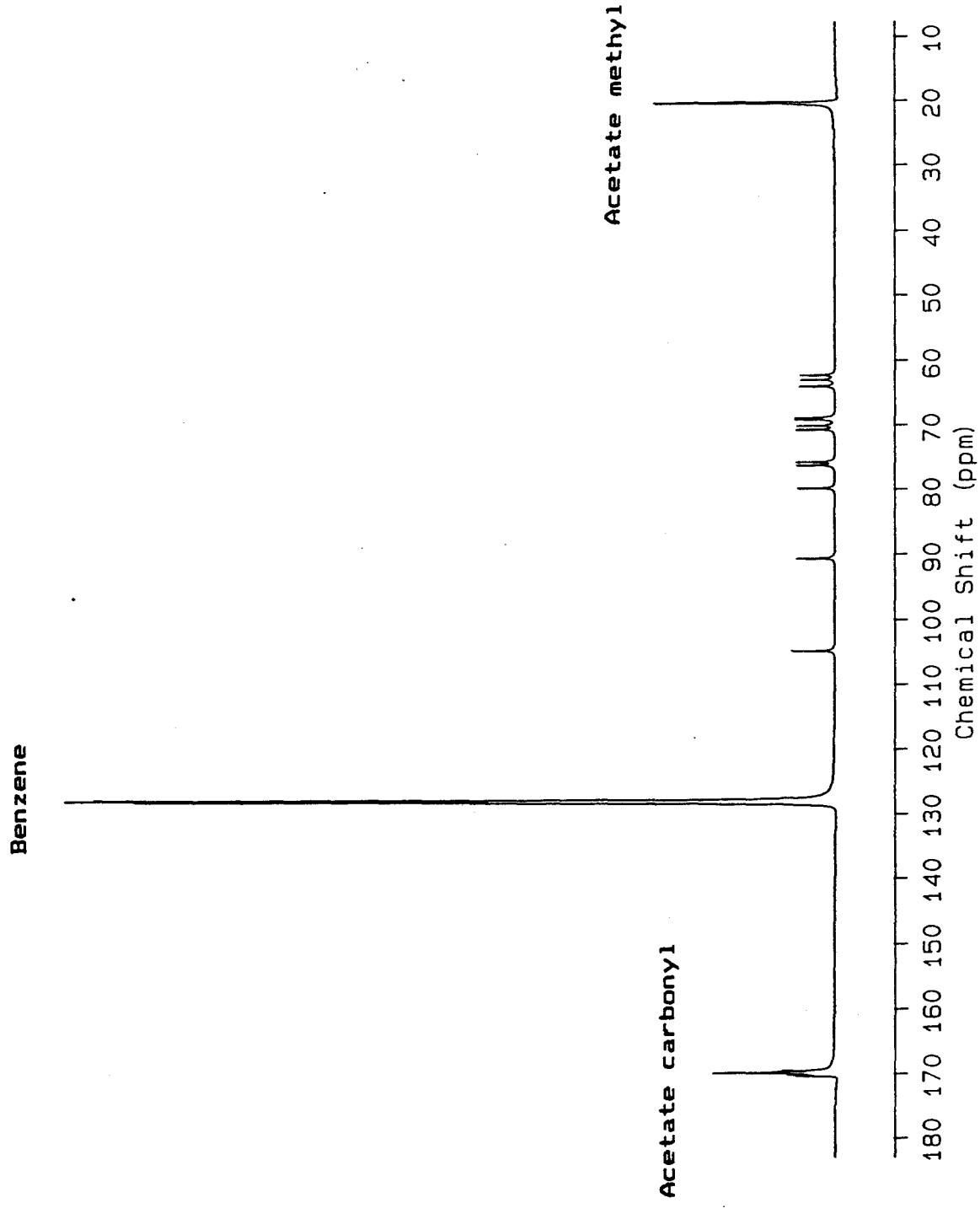

Figure 11. Spectrum of sucrose octaacetate in benzene-d6, acquired on the AM 500.

Table 5. Summary of % ^{13}C difference of cane and beet sugar in various measurements using glucose-C1 (G1) as the internal reference

	Pure cane vs. beet		Sugar mixing			Sugar octaacetate mixing
	(1)#	(2)#	(3)#	(4)#	(5)#	(6)#
	%	%	%	%	%	%
G1			Internal reference			
G2	2.2	-0.6	0.7	0.7	1.0	-0.1
G3	2.8*	-2.3	0.2	-1.1	-2.5	0.1
G4	2.4	-0.3	1.1	0	0.6	-0.8
G5	*	1.2	0.8	0.6	2.3	-0.4
G6	3.3	-0.7	0.8	1.4	1.8	0.5
F1	2.8	-1.2	0.6	1.4	1.0	0.6
F2	1.5	-0.2	0.5	-1.0	-0.4	-1.2
F3	-0.2	-1.3	0.6	-0.3	-0.9	0.1
F4	-0.3	-2.0	-0.2	-0.5	-1.5	-1.0
F5	-1.6	-0.7	-0.2	-0.7	-0.7	0.3
F6	1.7	-2.4	0.1	1.1	0	0.7

Notes- 1. Differences were found by subtracting relative peak height of beet from that of cane (or the two end points in mixing experiments)
2. G1-G6 and F1-F6 are carbons in the glucose and fructose unit respectively (See **Figure 6**)

* peaks were not fully resolved
# (1) Spectra acquired on Bruker AC 200
(2) Acquired on Bruker AMX 500
(3) Acquired on Bruker AM 500; CH_3CN as external reference
(4) Acquired on Bruker AMX 500; no reference was used
(5) FIDs from (4) processed by a PC package NMR286
(6) Acquired on AMX 500; acetate methyl as internal reference

Table 6. Summary of % ^{13}C difference of cane and beet sugar in various measurements using fructose-C5 (F5) as the internal reference

	Pure cane vs. beet		Sugar mixing			Sugar octaacetate mixing
	(1)	(2)	(3)	(4)	(5)	(6)
	%	%	%	%	%	%
G1	1.6	0.7	0.3	0.7	0.7	-0.3
G2	3.9	0.1	1.0	1.3	1.6	-0.5
G3	5.3*	-1.5	0.4	-0.4	-1.8	-0.3
G4	4.0	0.3	1.4	0.6	1.2	-1.2
G5	*	2.0	1.1	1.3	3.0	-0.7
G6	4.7	-0.2	1.1	1.9	2.4	0.2
F1	4.2	-0.7	0.8	1.8	1.6	0.3
F2	3.2	0.6	0.8	-0.2	0.3	-1.6
F3	1.4	-0.6	0.9	0.4	-0.2	-0.3
F4	1.3	-1.4	0	0.2	-0.8	-1.3
F5			Internal	reference		
F6	3.0	-2.0	0.2	1.5	0.5	0.4

Note - See **Table 5** for description of special features

Table 7. % ^{13}C difference of cane and beet sugar in the mixing experiments using methyl of CH_3CN and acetate methyl of octaacetate as reference

	Sugar mixing (CH_3CN as external reference) %	Sugar octacetate mixing (acetate methyl as internal reference) %
G1	9.9	0.3
G2	9.6	0.3
G3	9.7	-1.9
G4	10.7	0.2
G5	10.9	0.2
G6	7.9	0.4
F1	7.5	0.4
F2	11.0	0.1
F3	10.4	0.3
F4	9.0	0.1
F5	8.7	0.4
F6	6.4	0.4

sidebands might be produced and seen as extra signals in the spectrum. This would affect the accuracy of the peak height measurement if the sidebands overlapped with the sucrose signals. The artifacts were confirmed to be spinning sidebands because when beet octaacetate was run with spinning off (**Table 5**), these artifacts disappeared. Consequently, the rest of spectra were acquired without spinning. The resulting line-broadening caused by non-spinning was considered insignificant because the natural linewidth of carbon signals was quite broad and also a heavy line-broadening factor was usually used.

The spectra of this set of experiments showed that the phase of the peaks, especially that of benzene, acetate carbonyl and acetate methyl peaks, drifted from spectrum to spectrum (**Figure 11**). This was not a good sign since the reproducibility of spectra would be affected. The magnitude of the errors would depend on how severe the phase-drift was. Two speculations were made. Firstly, the benzene and acetate methyl signals had long T_1s. Even though Cr^{3+} had been added, the recycle time used (10 sec) might not be sufficient for these nuclei to fully relax. Secondly, phase anomalies might result if the decoupler power was insufficient to cause uniform and full proton decoupling. Incomplete relaxation would introduce phase errors whereas incomplete decoupling would cause variation in linewidths in addition to phase errors.

Experimentally, the delay time (D1) was increased to 20 then to 60 sec and the decoupler power (DP) was increased from 10H to 3H (**Table 5**). The results showed that at DP 3H, the linewidths of the carbon signals across the spectrum were most constant and narrow. A waiting time of 60 sec would likely be > 5 T_1. However, phase drifting

was still observed. Among the three, the benzene peak exhibited most severe phase drifting.

The spectral appearance of the benzene peak suggested that the phase-drift problem might be caused by the presence of solvent. Examination of sucrose octaacetate spectrum in solvents such as methanol, acetonitrile and acetone indicated that phase-drift was less severe when the spectra were acquired on the AC 200. This led to the third and fourth speculations: spectral effects due to the solvent or reference, and spectrometer instability.

The purpose of using sucrose octaacetate was to measure absolute difference of ^{13}C between cane and beet sugars with the use of the internal peak. The presence of the acetate methyl group in sucrose octaacetate served as an internal reference for the carbons in the sucrose skeleton. However, the solvents were very likely to cause unavoidable phase errors. This was why cane/beet mixing experiment was performed with CH_3CN as the external reference so that phase errors introduced by the solvent would be eliminated, but the purpose of getting absolute difference would be retained. Good precision ($\leq$ 0.5%, (3) in **Tables 8** and **9**) was obtained but the phase especially that of CH_3CN was seen drifting (**Figure 12**). This strengthened the idea that the solvent or the reference signal, CH_3CN in this case and C_6D_6 in sugar octaacetate, was too strong and it might have overloaded the digitizer (ADC) in the detector, thus causing dynamic range problems.

Table 8. Comparison of % standard deviation (%SD) of glucose-carbons from the calculation of average of ratios (AoR) and ratio of averages (RoA)

	G1	G2	G3	G4	G5	G6
(1) a.AoR(%)	0	0.7	0.8*	1.2	*	1.2
RoA(%)	1.8	2.0	1.6*	2.2		2.1
b.AoR(%)	0	1.7	1.3*	1.4	*	1.6
RoA(%)	1.2	1.4	1.2*	1.1		1.3
(2) a.AoR(%)	0	0.7	1.2	0.6	1.2	1.1
RoA(%)	0.8	0.8	1.6	0.8	1.1	1.0
b.AoR(%)	0	0.8	0.7	0.7	0.9	1.1
RoA(%)	0.8	0.6	1.1	0.7	0.8	1.0
(3) a.AoR(%)	0	0.3	0.5	0.3	0.3	0.5
RoA(%)	1.2	1.4	1.1	1.3	1.4	1.4
b.AoR(%)	0	0.3	0.3	0.3	0.5	0.5
RoA(%)	1.3	1.2	1.1	1.1	1.1	1.5
(4) a.AoR(%)	0	0.3	0.2	0.3	0.3	0.6
RoA(%)	0.8	0.7	0.9	0.7	0.7	0.7
b.AoR(%)	0	0.4	0.5	0.5	0.5	0.5
RoA(%)	0.8	0.5	1.0	0.5	0.5	0.5
(5) a.AoR(%)	0	0.4	0.3	0.3	0.3	0.5
RoA(%)	0.6	0.5	0.8	0.5	0.5	0.5
b.AoR(%)	0	0.5	0.6	0.6	0.7	0.7
RoA(%)	0.6	0.5	1.1	0.5	0.6	0.6
(6) a.AoR(%)	0	0.2	0.4	0.4	0.1	0.2
RoA(%)	0.5	0.4	0.4	0.7	0.4	0.5
b.AoR(%)	0	0.3	0.4	0.5	0.6	0.8
RoA(%)	2.4	2.3	2.5	2.2	2.1	2.9

Notes- 1. See **Table 5** for description of special features
2. a. %SD of cane carbons
b. %SD of beet carbons

Table 9. Comparison of % standard deviation (%SD) of fructose-carbons from the calculation of average of ratios (AoR) and ratio of averages (RoA)

	F1	F2	F3	F4	F5	F6
(1) a.AoR(%)	1.2	1.4	1.1	1.3	1.7	0.9
RoA(%)	1.7	2.0	2.1	1.7	2.0	1.9
b.AoR(%)	1.4	1.6	1.4	1.2	1.2	1.6
RoA(%)	1.4	1.5	1.4	1.4	1.4	1.4
(2) a.AoR(%)	0.5	0.4	0.4	0.8	0.3	0.7
RoA(%)	0.7	0.9	1.0	1.2	0.9	1.1
b.AoR(%)	0.7	0.5	0.3	0.5	0.2	0.7
RoA(%)	0.7	0.5	0.8	0.8	0.8	0.8
(3) a.AoR(%)	0.3	0.3	0.3	0.3	0.2	0.4
RoA(%)	1.3	1.2	1.3	1.3	1.2	1.4
b.AoR(%)	0.4	0.4	0.4	0.3	0.3	0.5
RoA(%)	1.3	1.3	1.4	1.4	1.3	1.3
(4) a.AoR(%)	0.5	0.2	0.3	0.3	0.2	0.4
RoA(%)	0.6	0.8	0.8	0.7	0.8	0.7
b.AoR(%)	0.4	0.3	0.2	0.3	0.2	0.2
RoA(%)	0.5	0.5	0.7	0.9	0.6	0.6
(5) a.AoR(%)	0.4	0.2	0.2	0.2	0.2	0.3
RoA(%)	0.5	0.6	0.7	0.6	0.6	0.7
b.AoR(%)	0.4	0.1	0.3	0.5	0.2	0.3
RoA(%)	0.5	0.5	0.8	0.9	0.6	0.6
(6) a.AoR(%)	0.1	0.3	0.3	0.2	0.2	0.2
RoA(%)	0.5	0.5	0.4	0.5	0.4	0.4
b.AoR(%)	0.8	1.4	0.7	1.0	0.5	0.7
RoA(%)	2.9	2.0	2.1	2.0	2.7	2.8

Note - See **Table 5** and **Table 8** for description of special features

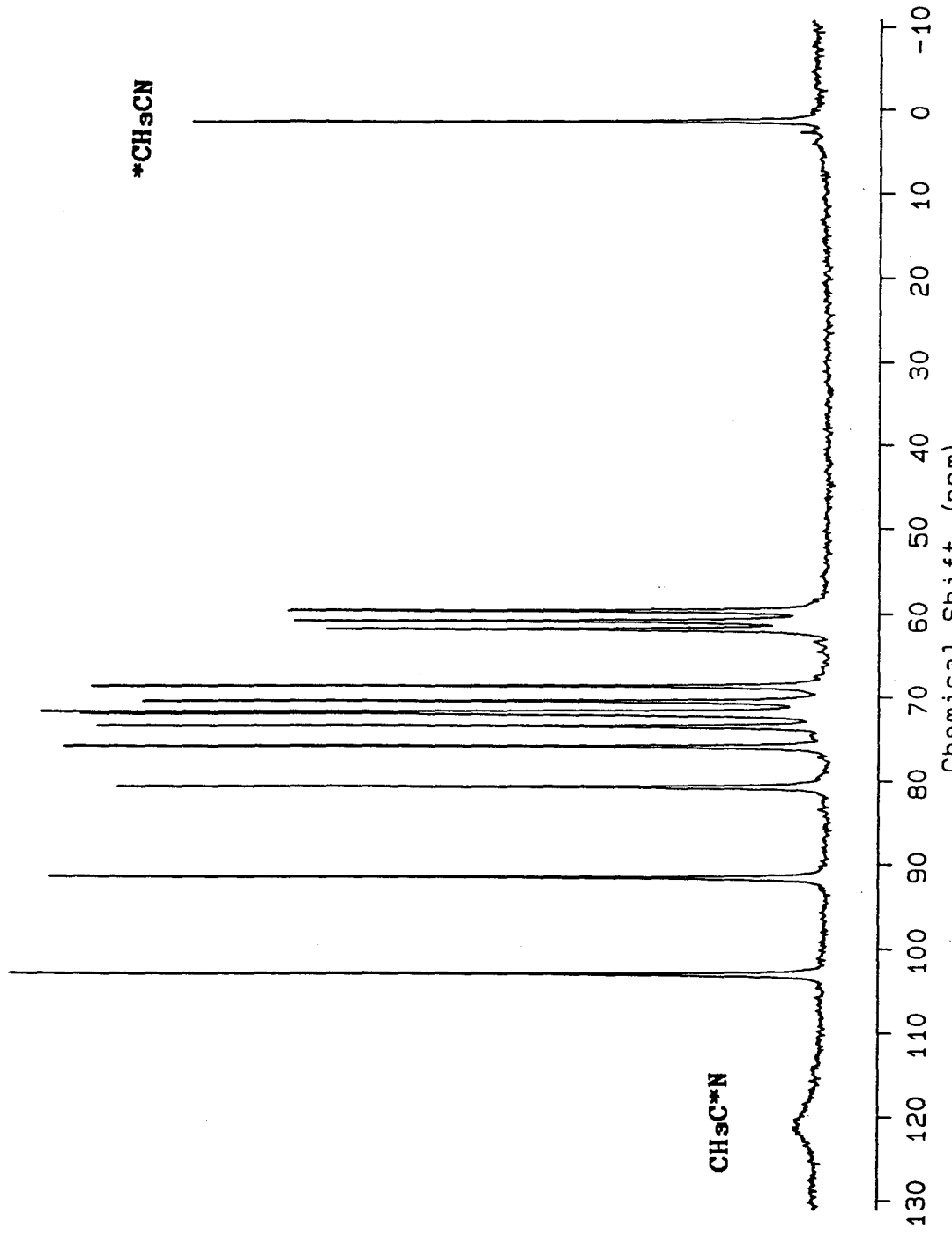

Figure 12. Spectrum of sucrose obtained from the mixing experiment, acquired on the AM 500.

To tackle the phase-drift problem, no external reference was used when pure sucrose was run on the AC 200. The phase of the peaks was less drifting. This was evident of the presence of dynamic range problem caused by the strong solvent signal.

The fluctuations in precision found in the above experiments ((1), (3) and (6) in **Tables 8** and **9**) also suggested that spectrometer instability was a possible error source. In data analysis, the block-averaging program NMRSTAT was used to obtain the average and the standard deviation (SD) spectra. It was seen in some of the SD spectra that peaks split into two humps resulting in a rise of SD at the wings of the peaks (**Figure 13**). This was a sign of the existence of not only the drifting phase but also the electronic fluctuations of the spectrometer. NMRSTAT is a statistical program providing the averages and the associated uncertainty in the form of spectrum. The height of each point (or the location) in an SD peak corresponds to the error of the same location in the average peak. An SD peak therefore reflects the degree of variation in the peak shape (peak width and phase). In other words, the rise in the wings indicated that higher uncertainty was found at the wings of the signal. This was very likely a consequence of the drifting phase of the spectra in the same block, caused by the solvent effect. Similar effect might result if the transmitter power was not stable enough to stabilize the frequency of the deuterium lock signal or the receiver could not maintain same lock phase. The duration to acquire a block of spectra was ~ 10 hours. It would be possible that the spectral appearance suffered from a loss of stability. As is seen in the same figure, it is the dip of the standard deviation peak which matches the vertex of the average peak. This would suggest that although phase drift did contribute to the total

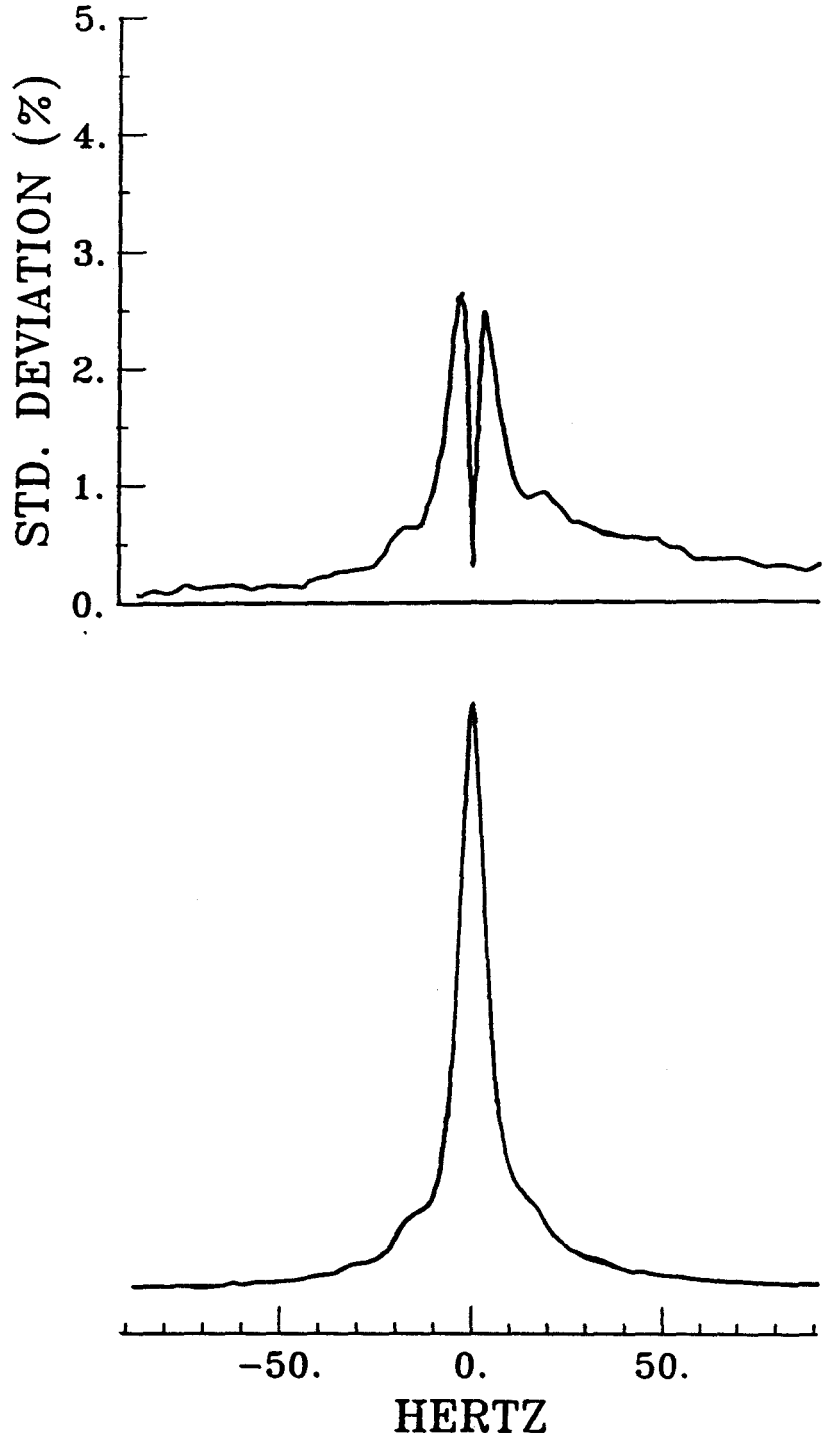

Figure 13. A split standard deviation peak with the dip matched with the vertex of the corresponding average peak, extracted from a ^{13}C NMRSTAT spectrum.

error, but the peak height was less susceptible to the effect.

It was possible that the aging of the local spectrometers would downgrade the precision of the spectra. As part of the precautions as well as a step to find out the limit of the method, two sets of samples were run on a more stable FT spectrometer (Bruker AMX 500).

Comparing the %SD in **Tables 8** and **9**, it is obvious that the use of 500 MHz spectrometers ((2), (3), (4) and (6)) resulted in three- or four-fold reduction of the standard deviations than the 200 MHz spectrometer (1). Data analysis also showed that the different ways of computing the averages and standard deviations resulted in different error magnitude. Except for (1b), The trend was very consistent in the way that the average of ratios from block averaging always produced smaller standard deviations than the ratio of averages. Three- to five-fold improvement was common in these results. The smallest standard deviation by far is 0.1 % as seen in (6a). The most frequent occurrence is 0.3 %.

The standard deviations of sucrose octaacetate mixing experiment (6b), especially those associated with RoA, are unusually high when compared to the rest. It was noticed that the peak height of the signals in the third spectrum of the block were general smaller. When AoR were taken, the variation was ratioed out, resulting in smaller error magnitude. However, when RoA were taken, the variation contributed to higher uncertainty and showed up in the final standard deviation. This observation strongly suggests that the average of ratios would be more advantageous than the ratio of averages.

In order to see whether there were operator biases involved in spectrum

processing, the mixing sugar spectra run and processed on the AMX 500 were re-processed with NMR286 by a second operator. During the processing, no baseline correction or any other lineshape correction were made. The results ((4) and (5) in **Tables 5-9**) show that patterns in the averages and standard deviations are very similar. Although there is only one such set of comparison, the observed pattern would suggest that personal biases had no effect, at least on this occasion.

Focus has been put on the precision term in the above discussion. This is so because how effective NMR can be in doing quantitation and how feasible the peak height method is relies heavily on the precision of block averaging. However, it is also true that the accuracy of the results cannot be ignored.

As mentioned in the Introduction, cane sugar has a higher ^{13}C content than beet sugar. Experimentally, the difference was measured by either the external or internal referencing method. Since phase-drift was observed when an external reference or a derivative peak was used, it was more reliable to use a sucrose peak as the internal reference. Both G1 and F5 were used as the internal reference since they did not overlap with other peaks in the sucrose spectrum. As can be seen from **Tables 5, 6** and **7**, the pattern of the ^{13}C difference cannot be predicted because the trend is not consistent among different measurements. However, if taking the two extreme data points which belonged to pure cane and beet, site-specific effects are seen ($\geq$ 1% ^{13}C difference). **Table 10** presents the magnitude and standard deviation of the slopes of the carbon lines in the two mixing experiments obtained by using regression analysis. Only peak heights relative to G1 were analyzed. Four of the carbon lines are shown in **Figures 14** and **15**. In spite

of the sort of linearity shown by some carbon lines, no promising trend was established. For some lines (F1, F2, F4, G2), the discrepancy of the same carbon line in the two measurements is very large.

To conclude this section, it is possible to obtain a precision less than 0.5 % by using the peak height method provided that precautions and care are taken. The biggest problem encountered in the experimental section was the phase-drift. Experimental results showed that the use of solvent or derivative peak was very likely to cause dynamic range problem, thus producing phase anomalies. The stability and resolution of a spectrometer was also found to affect the precision. The use of the average of ratios is certainly more advantageous than the ratio of averages in reducing the error magnitude of the relative peak heights. The results at this stage is quite preliminary. More studies are needed to see whether the site-specific isotope effects exist.

Table 10. Slopes and standard deviations from linear regression analysis for the carbon lines in the sugar mixing (CH_3CN as the external reference) and the sugar octaacetate experiments.

	Sugar mixing			Sugar octaacetate mixing		
	Slope	SD*	% SD#	Slope	SD*	% SD#
G2	0.008	0.003	38	-0.001	0.001	122
G3	0.005	0.007	157	0	0.002	551
G4 (x)	0.010	0.002	21	-0.008	0.001	14
G5	0.010	0.004	38	-0.003	0.001	24
G6 (□)	0.006	0	6	0.006	0.001	20
F1	0.002	0.004	256	0.007	0.003	40
F2 (+)	0	0.007	2164	-0.010	0.003	31
F3 (■)	0.003	0.004	126	0.001	0.001	59
F4	-0.003	0.005	144	-0.009	0.001	14
F5	0.001	0.004	775	0.003	0.002	77
F6	0.010	0.003	29	0.004	0.001	17

Note:- The lines of G4, G6, F2 and F6 are shown in **Figures 14** and **15**. Each symbols represents the marker of the line.

* Absolute standard deviation of the slope
# Percentage standard deviation of the slope

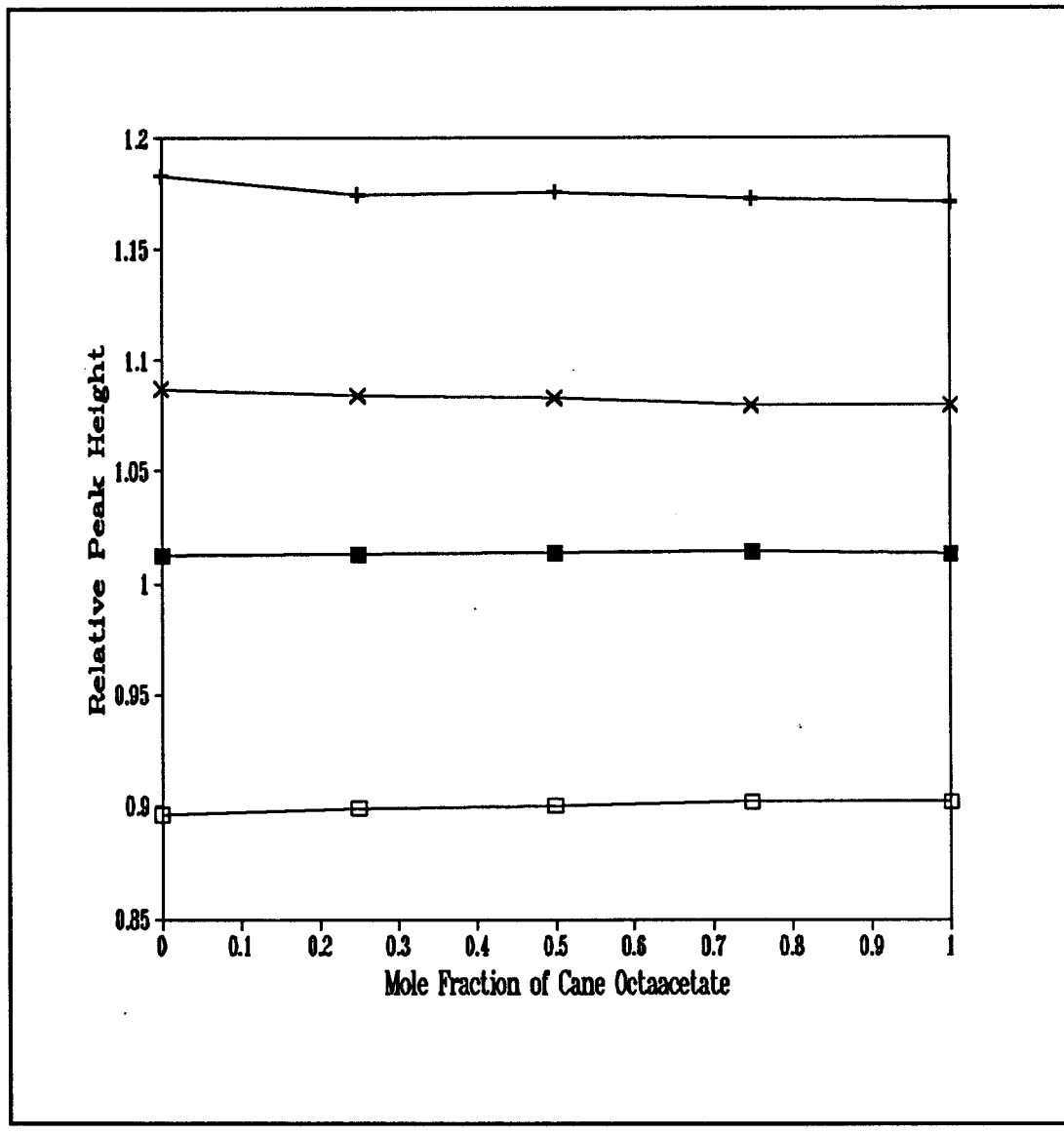

Figure 14. Correlation of the relative peak heights to the mole fraction of cane sugar octaacetate. G1 is the reference peak. Two carbon lines are from the glucose unit and the other two from the fructose unit: F2 (+), F3 (■), G4 (x) and G6 (□)

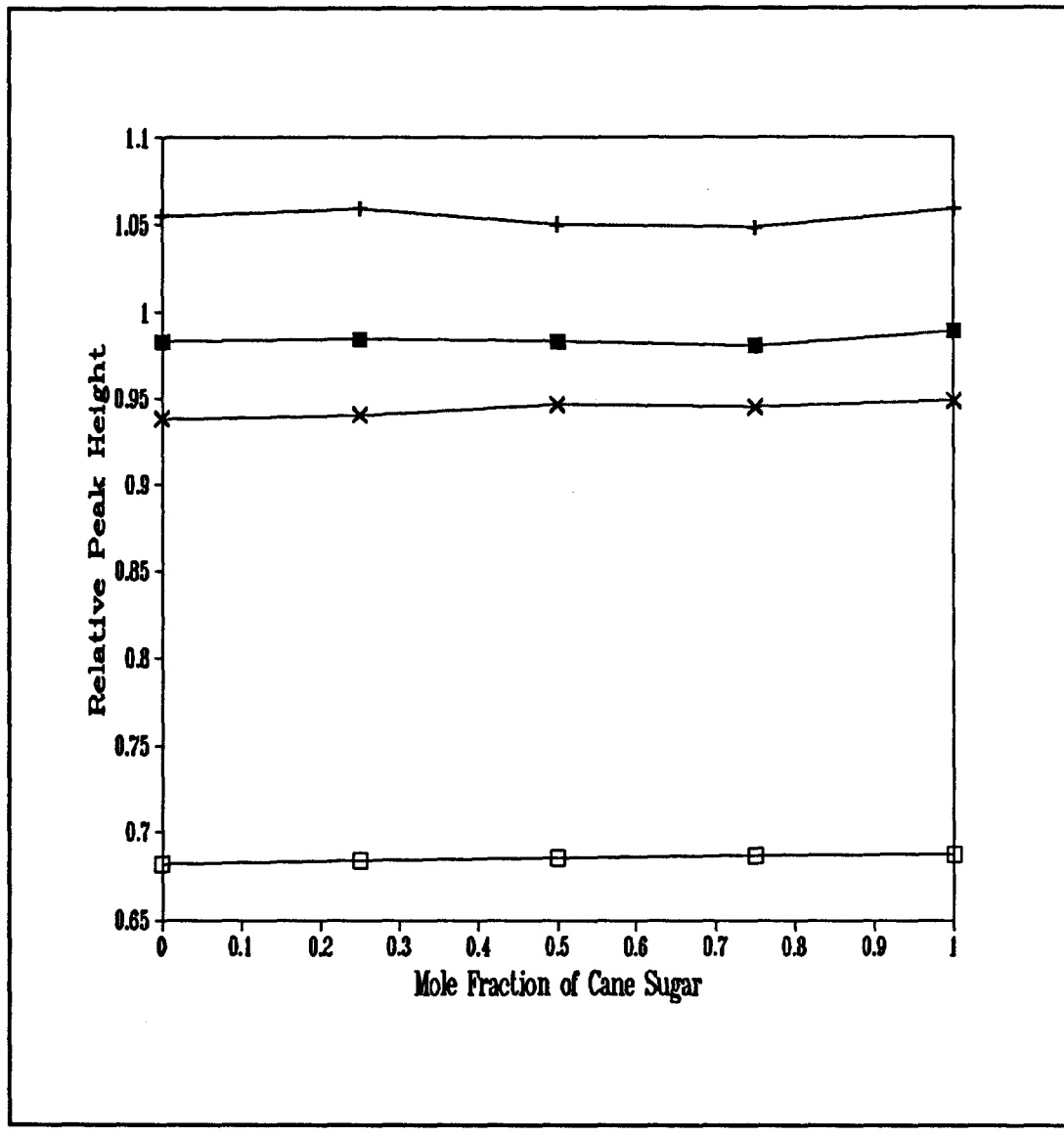

Figure 15. Correlation of the relative peak heights to the mole fraction of cane sugar from the sugar mixing experiment (CH_3CN as the external reference). G1 is the reference peak. The carbon lines are: F2 (+), F3 (■), G4 (x) and G6 (□).

CHAPTER 6 CONCLUSION

Firstly, it has been demonstrated in the deuterium work the success of using the peak height method in quantitative ^{2}H NMR. The linearity of the established model was validated and the applicability was also proved in the analysis of DMSO/water mixtures. As well, the use of samples with known concentration provided a very effective way to check the precision of the method and the accuracy of the experimental data.

Secondly, both discouraging and encouraging results have been obtained from the ^{13}C work. The objective to seek any site-specific information of the sucrose carbons has not been fulfilled. It was found that some carbons in cane and beet sugars exhibited different amount of ^{13}C. This seemed to be a sign of the existence of site-specific isotope enrichment. However, the pattern of the ^{13}C difference was so inconsistent that no definite conclusion could be drawn. On the other hand, excellent precision of the relative peak heights were obtained for most of the carbon data. It was usually about 0.3 to 0.5 % with several down to 0.2 %. With this kind of precision, the peak height method would be considered reliable.

6.1 Remarks on the Statistical Analysis:

1. Block averaging enables the computation of the standard deviation for spectra that

belong to the same block. This in turn provides a means to evaluate the reproducibility of the peak heights.

2. Relative peak heights have played a key role in data analysis. Its usefulness has been demonstrated in the water experiments in the way that constant biases could be eliminated.
3. As a complement to 2., the precision of the relative peak heights can be further improved by taking the average of ratios rather than the ratio of averages. The sucrose data has shown that even variations existed in the raw peak heights, the effect on the precision was counteracted when the approach of calculating the average of ratios was used, without changing the value of the averages.

6.2 Suggestions for Future Work:

1. All deuterium spectra of water and water mixtures were acquired on the 250 MHz spectrometer. A more stable spectrometer might improve the precision of the raw peak heights.
2. Regarding the referencing methods used in the sucrose work, less phase problems were encountered for CH_3CN than for methyl acetate in sucrose octaacetate. More work can be done on using other external references to get rid of the phase drift. Of course, to be a qualified reference, the peak signal should be well resolved and has comparable signal strength.
3. Both accuracy and precision have been attained in the quantitative ^2H measurements.

It is suggested that studies are aimed to see whether (a) the precision obtained in both ^{2}H and ^{13}C work is the real limit of the NMR methods; (b) the peak height method is applicable to ^{13}C analysis; and (c) the method can be applied to analyze other nuclei.

REFERENCES

1. D. Shaw, *Fourier Transform N. M. R. Spectroscopy*, Elsevier, Amsterdam, 1976.

2. M.L. Martin, J.-J. Delpuech and G.J. Martin, *Practical NMR Spectroscopy*, Heyden, London, 1980.

3. R.R. Ernst, G. Bodenhausen and A. Wokaun, *Principles of Nuclear Magnetic Resonance in One and Two Dimensions*, Clarendon Press, Oxford, 1987.

4. J.K.M. Sanders and B.K. Hunter, *Modern NMR Spectroscopy. A Guide for Chemists*, Oxford University Press, Oxford, 1988.

5. A.E. Derome, *Modern NMR Techniques for Chemistry Research*, Pergamon Press, Oxford, 1988.

6. L.D. Field and S. Sternhell (eds.), *Analytical NMR*, J. Wiley, Chichester, 1989.

7. A.D. Bain and L.Lao, in *Isotopes in the Physical and Biochemical Sciences*, E. Buncel and J. R. Jones, eds., Elsevier, Amsterdam, (in press).

8. R. Freeman and G.A. Morris, *Bull. Magn. Reson.* **1**, 1 (1979).

9. W.R. Croasmun and R.M.K. Carlson (eds.), *Two-Dimensional NMR Spectroscopy*, VCH Publishers, New York, 1987.

10. R. Damadian, *Philos. Trans. R. Soc. London* **289**, 489 (1980).

11. J.M.S. Hutchison, W.A. Edelstein and G.A. Johnson, *J. Phys. Instrum.* **13**, 947 (1980).

12. P.G. Morris, *Nuclear Magnetic Resonance Imaging in Medicine and Biology*, Clarendon Press, Oxford, 1985.

13. F.W. Wehrli, D. Shaw and J.B. Kneeland, *Biomedical Magnetic Imaging, Principles, Methodology and Applications*, VCH Publishers, New York, 1988.

14. D.L. Turner, *Recent Developments in Multiple Pulse NMR* in *Annual Reports on NMR Spectroscopy*, Volume 21, G. A. Webb, ed., Academic Press, London, 1989.

15. J.C. Randall and E.T. Hsieh, *ACS Symposium Series* **247**, 131 (1984).

16. R. Chujo, Y. Tanaka, Y. Terawaki, K. Hatada, T. Kitayama, R. Kitamaru, F. Horii and H. Sato, *Polymer J.* **20**, 627 (1988).

17. A.E. Tonelli, *NMR Spectroscopy and Polymer Microstructure: The Conformational Connection*, VCH Publishers, New York, 1989.

18. J.K. Kwakye, *Talanta* **32**, 1069 (1985).

19. K. Wüthrich, *NMR of Proteins and Nucleic Acids*, J. Wiley, New York (1986).

20. J.H. Battocletti, *CRC Crit. Rev. Biomed. Eng.* **7**, 44 (1986).

21. P.W. Kuchel, *Biological Applications of NMR* in *Ref.* 6.

22. H.-O. Kalinowski, S Berger and S. Braun, *Carbon-13 NMR Spectroscopy*, J. Wiley, New York (1988).

23. V.J. Robinson, A.D. Bain and C.A. Rodger, *Steroids* **48**, 267(1986).

24. L.A.C. Pieters and A.J. Vlietinck, *J. of Pharm. Biomed. Anal.* **7**, 1405 (1989).

25. C. Rabiller and F. Maze, *Magn. Reson. Chem.* **27**, 582(1989).

26. A. Rapp, E. Hupfer, M. Spraul and A. Markowetz, *Z. Lebensmityel Untersuch. Forsch.* **188**, 138 (1989).

27. E. Murphy, L. Levy, B. Raju, C. Steenbergen, J.T. Gerig, P. Singh and R.E. London, *Env. Health Persp.* **84**, 95 (1990).

28. Z. Glowacki, M. Topolski, E. Matczak-Jon and M. Hoffman, *Magn. Reson. Chem.* **27**, 922 (1989).

29. J.L. Evelhoch, B.P. Gini and C.L. McCoy, *Magn. Reson. Med.* **9**, 402 (1989).

30. G.C. Levy, T. Pehk and P.R. Srinivasan, *J. Magn. Reson.* **14**, 129 (1980).

31. W. Schilf, L. Stefaniak, G.A. Webb and M. Witanowski, *J. Mol. Struct.* **140**, 311 (1986).

32. H. Molinari and S. Mammi, *J. Magn. Reson.* **90**, 355 (1990).

33. S. Fujiwara, Y. Yano and K. Nagashima, *Chem. Instrum.* **2**, 103 (1969).

34. K. Hatada, Y. Terawaki, H. Okuda and H, Yuki, *Anal. Chem.* **41**, 1518 (1969).

35. F. Bloch, W.W. Hansen and M. Packard, *Phys. Res.* **70**, 474 (1946).

36. H.C. Torrey, *Phys. Res.* **76**, 1059 (1949).

37. E.L. Hahn, *Phys. Res.* **80**, 580 (1951).

38. R.R. Ernst and W.A. Anderson, *Res. Sci. Instrum.* **37**, 93 (1966).

39. J.B.J. Fourier, *Theorie Analytique de la Chaleur*, Paris, 1822.

40. J.W. Cooley and J.W. Tukey, *Math. Comput.* **19**, 297 (1965).

41. M. Spraul, *Automatic NMR Analysis* in *Ref.* 6.

42. F. Kasler, *Quantitative Analysis by NMR Spectroscopy*, Academic Press, London, 1973.

43. D.E. Leyden and R.H. Cox, *Analytical Applications of NMR*, J. Wiley, New York, 1977.

44. J.N. Shoolery, *Varian Application Note*, NMR-73-4, Varian, Palo Alto, CA, 1974.

45. J.N. Shoolery, *Prog. Nucl. Magn. Reson. Spectrosc.* **11**, 79 (1977).

46. T.H. Mareci and K.N. Scoott, *Anal. Chem.* **49**, 2130 (1977).

47. J. Hinton, M. Oka and A. Fry, in *Isotopes in Organic Chemistry*, Volume 3, E. Buncel and C.C. Lee, eds., Elsevier, Amsterdam, 1977.

48. C.H. Sotak, C.L. Dumoulin and G.C. Levy, in *Topics in Carbon-13 NMR Spectroscopy*, Volume 4, G. C. Levy, ed., J. Wiley, New York, 1894.

49. J.R. Mooney, *Quantitative Applications of ^{13}C NMR* in *Ref.* 6.

50. G.J. Martin and M.L. Martin, *Tetrahedron Lett.* **22**, 3525 (1981).

51. G.J. Martin, M.L. Martin and F. Mabon, *J. Am. Chem. Soc.* **104**, 2658 (1982).

52. G.J. Martin, M.L. Martin, F. Mabon and M.-J. Michon, *J. Chem. Soc., Chem. Commun.*, 616 (1982).

53. G.J. Martin, M.L. Martin, F. Mabon and M.-J. Michon, *Anal. Chem.* **54**, 2380 (1982).

54. G.J. Martin and N. Naulet, *Fresenius Z. Anal. Chem.* **332**, 648 (1988).

55. C. Guillou, M. Trierweiler and G.J. Martin, *Magn. Reson. Chem.* **26**, 491 (1988).

56. R.A. Pascal, Jr., M.W, Baum, C.K. Wagner and L.R. Rodgers, *J. Am. Chem. Soc.* **106**, 5377 (1984).

57. R.A. Pascal, Jr., M.W. Baum, C.K. Wagner, L.R. Rodgers and D.-S. Huang, *J. Am. Chem. Soc.* **108**, 6477 (1986).

58. B.-L. Zhang, *Magn. Reson. Chem.* **26**, 955 (1988).

59. S. Gillet and J.-J. Delpuech, *J. Magn. Reson.* **38**, 433 (1980).

60. D.J. Cookson and B.E. Smith, *J. Magn. Reson.* **57**, 355 (1984).

61. F.A.L. Anet and D.J. O'leary, *Tet. Lett.* **30**, 1059 (1989).

62. R. Aydin and H. Günther, *Angew. Chem., Int. Ed. Engl.* **20**, 985 (1981).

63. G.A. Ward and R.D. Mair, *Anal. Chem.* **41**, 538 (1969).

64. K. Schaumburg, *Lipids* **5**, 505 (1970).

65. I.M. Armitage, H. Huber, D.H. Live, H. Pearson and J.D. Roberts, *J. Magn. Reson.* **15**, 142 (1974).

66. S. Sibisi, J. Skilling, R.G. Brereton, E.D. Laue and J. Staunton, *Nature* **311**, 446 (1984).

67. B.J. Fahie and W.J. Leigh, *Can. J. Chem.* **67**, 1859 (1989).

68. S. Fujiwara, Y. Yano and K. Nagashima, *Chem. Instrum.* **1**, 103 (1969).

69. R. Freeman, *A handbook of Nuclear Magnetic Resonance*, Longman, Britain, 1988.

70. W. Pauli, *Naturwiss.* **12**, 741 (1924).

71. R.K. Harris and R.H. Newman, *J. Magn. Reson.* **24**, 449 (1976).

72. A.W. Overhauser, *Phys. Rev.* **89** (1953).

73. I. Solomon, *Phys. Rev.* **99**, 559 (1955).

74. J.H. Noggle and R.E. Schirmer, *The Nuclear Overhauser Effect*, Academic Press, New York, 1971.

75. D. Neuhaus and M.P. Williamson, *The Nuclear Overhauser Effect in Structural and Conformational Analysis*, VCH Publishers, New York, 1989.

76. J. McConnell, *The Theory of Nuclear Magnetic Relation in Liquids*, Cambridge University Press, Cambridge, 1987.

77. G.C. Levy and J.D. Cargioli, *J. Magn. Reson.* **10**, 231 (1973).

78. R.R. Ernst and R.E. Morgan, *Mol. Phys.* **26**, 49 (1973).

79. R. Freeman, H.D.W. Hill and R. Kaptein, *J. Magn. Reson.* **7**, 327 (1972).

80. J.W. Cooper, *J. Magn. Reson.* **22**, 345 (1976).

81. J.W. Cooper, *J. Magn. Reson.* **28**, 405 (1977).

82. J.W. Cooper, in *Topics in Carbon-13 NMR Spectroscopy*, Volume 2, G. C. Levy, ed., J. Wiley, New York, 1976.

83. R.R. Ernst, *J. Chem. Phys.* **45**, 3845 (1966).

84. H.-C. Chiang and L.-J. Lin, *Org. Magn. Reson.* **12**, 260 (1979).

85. J. Tamate and J.H. Bradbury, *J. Sci. Food Agric.* **36**, 1291 (1985).

86. S.T. Eberhart, A Hatzis and Rothchild, *J. Pharm. Biomed. Anal.* **4**, 147 (1986).

87. M.A. Sharaf, D.L. Illman and B.R. Kowalski, *Chemometrics*, J. Wiley, New York, 1986.

88. D.L. Massart, B.G.M. Vandeginste, S.N. Deming, Y. Michotte and L. Kaufman, *Chemometrics: A Textbook*, Elsevier, Amsterdam, 1988.

89. P. de Bièvre, *Adv. Mass Spectrom.* **7A**, 385 (1978).

90. D.L. Hachey, W.W. Wong, T.W. Boutton and P.D. Klein, *Mass Spectrom. Rev.* ,6 289 (1987).

91. R.S. Tse, S.C. Wong and C.P. Yuen, *Anal Chem.* **52**, 2445 (1980).

92. G.J. Martin, M.L. Martin and F. Mabon, *J. Am. Chem. Soc.* **104**, 2658 (1982).

93. G.J. Martin, P. Dupuy, M.L. Martin and B.-L. Zhang, *Biochem. Biophys. Res. Commun.* **3**, 890 (1983).

94. G.J. Martin, X.Y. Sun, C. Guillou and M.L. Martin, *Tetrahedron* **41**, 3285 (1985).

95. G.J. Martin, M. Benbernou and F. Lantier, *J. Inst. Brew.* **91**, 242 (1985).

96. G.J. Martin, P. Janvier and F. Mabon, *Analusis* **13**, 267 (1985).

97. G.J. Martin, P. Janvier, S. Akoka, F. Mabon and J. Jurczak, *Tetrahedron Lett.* **27**. 2855 (1986).

98. G.J. Martin, B.-L. Zhang, N. Naulet and M.L. Martin, *J. Am. Chem. Soc.* **108**, 5116 (1986).

99. C. Maubert, F. Mabon, C. Guerin and G.J. Martin, *Analusis* **16**, 434 (1988).

100. G.J. Martin, M.L. Martin, C. Guillou, M.T. Cabanis, J. Aerny and Y. Tep, *J. Agri. Food Chem.* **36**, 316 (1988).

101. M. Hajek and G.J. Martin, *Chemicke Listy* **83**, 404 (1989).

102. J.M. Franconi, G.J. Martin and N. Naulet, *J. C. S.* **10**, 69 (1989).

103. H. Graig, *Science* **133**, 1833 (1961).

104. G. Gonfiantini, *Nature (London)* **271**, 534 (1978).

105. T. Akazawa and K. Okamoto, in *The Biochemistry of Plants. A Comprehensive Treatise*, Volume 3, J. Preiss, ed., Academic Press, New York, 1980.

106. M.D. Hatch and N.K. Boardman, eds., *The Biochemistry of Plants. A Comprehensive Treatise*, Volume 8, Academic Press, New York, 1981.

107. G. Edwards and D. Walker, *C_3, C_4: Mechanisms, and Cellular and Environmental Regulation, of Photosynthesis*, University of California Press, Berkeley, 1983.

108. M.M. Bender, *Phytochemistry* **10**, 1239 (1971).

109. M.H. O'Lneary, *Phytochemistry* **20**, 553 (1981).

110. R.P. Linstead, A. Rutenberg, W.G. Dauben and W.L. Evans, *J. Am. Chem. Soc.* **62**, 3260 (1940).